COLOUR online, B&W in print

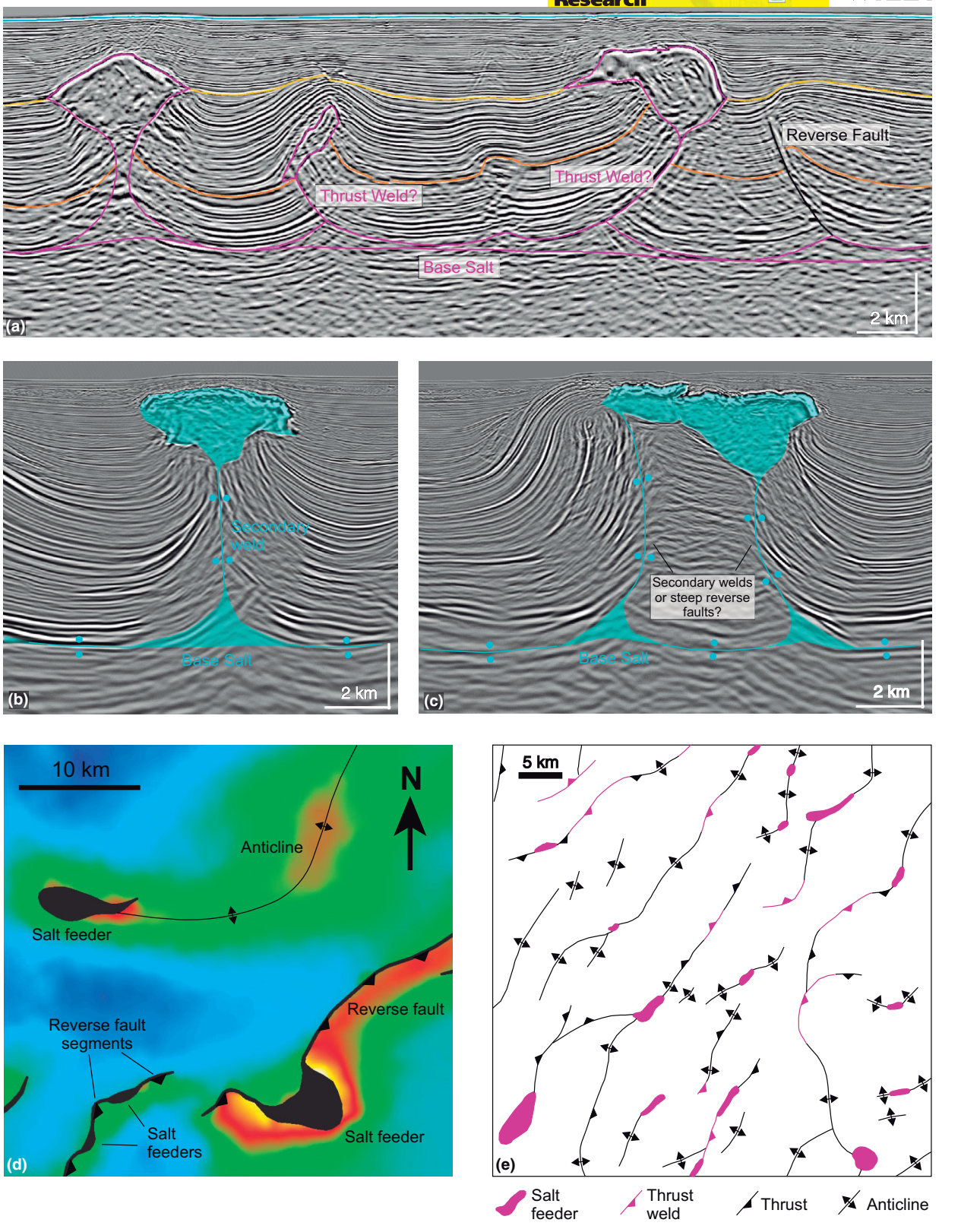

FIGURE 1 Salt diapirs and contractional structures: (a) Seismic section across the Sureste Basin in the southern Gulf of Mexico (data courtesy of WesternGeco) showing a series of squeezed diapirs, thrust welds and thrust faults detached on salt; (b) vertical weld from the southern Gulf of Mexico (Rowan, 2020; data courtesy of WesternGeco); (c) steep thrust welds with common footwall from the southern Gulf of Mexico (Rowan, 2020; data courtesy of WesternGeco); (d) depth-structure map from the northern Gulf of Mexico showing thrusts and folds merging into and linking squeezed diapirs (reds and yellows are highs, diapirs and linked thrusts are in black; modified from Rowan & Ratliff, 2012); (e) map of broadly linear structures in the southern Gulf of Mexico that comprise linked combinations of squeezed diapirs, vertical welds, thrust welds, thrust faults and salt-cored anticlines (shown with permission of WesternGeco)

The Warraweena area of the Northern Flinders (Figure 2) provides an excellent natural laboratory to investigate contractional salt tectonics at the sub-seismic scale and to answer the following questions: (a) What is the nature of the lateral transition from diapir to linking structures? (b) Are these linking features thrust welds or just thrusts? (c) If thrust welds, were they pre-existing diapirs that were squeezed shut or did the diapirs form only during shortening? (d) If thrusts, how does the geometry transition laterally from a remnant diapir to a thrust? (e) Is there any variation in structural style and stratal geometries between areas adjacent to diapirs or thrusts? (f) What kinds of small-scale deformation (fractures, shear, etc.) are present and how do they change along strike within the transition zone? (g) Might any such differences impact reservoir quality (i.e. secondary porosity or porosity reduction), trap configuration or hydrocarbon migration? The results of our study are relevant to those companies and institutions invested in exploration and production in fold-and-thrust belts with salt diapirs, such as the passive-margin basins of the Gulf of Mexico, the Lower Congo Basin and offshore Brazil, as well as convergent-margin basins such as the Austrian Alps and the Dinarides/Albanides/Hellenides in the Balkans.

2 | GEOLOGICAL SETTING

The Northern Flinders Ranges are located in the Adelaide Fold Belt, also known as the Adelaide Geosyncline or Adelaide Basin (Jenkins, 1990; Preiss, 1987, 2000; Sprigg, 1952; Thomson, 1969). The Adelaide Fold Belt is a broadly N-S trending fold belt extending ca. 700-km north from Kangaroo Island in South Australia (Figure 2) that evolved for at least 300 million years. The stratigraphic record is characterised by a >15-km-thick succession of Neoproterozoic and Cambrian rocks, including a basal remnant evaporite sequence, deposited during multiple phases of rifting (polyphase aulacogen) followed by shortening (Delamerian Orogeny). The aulacogen developed as western Laurentia separated from Australia during the breakup of the Rodinian supercontinent (Preiss, 2000). Basin inversion followed during the Delamerian Orogeny, which is variably considered to have taken place during the Late Cambrian

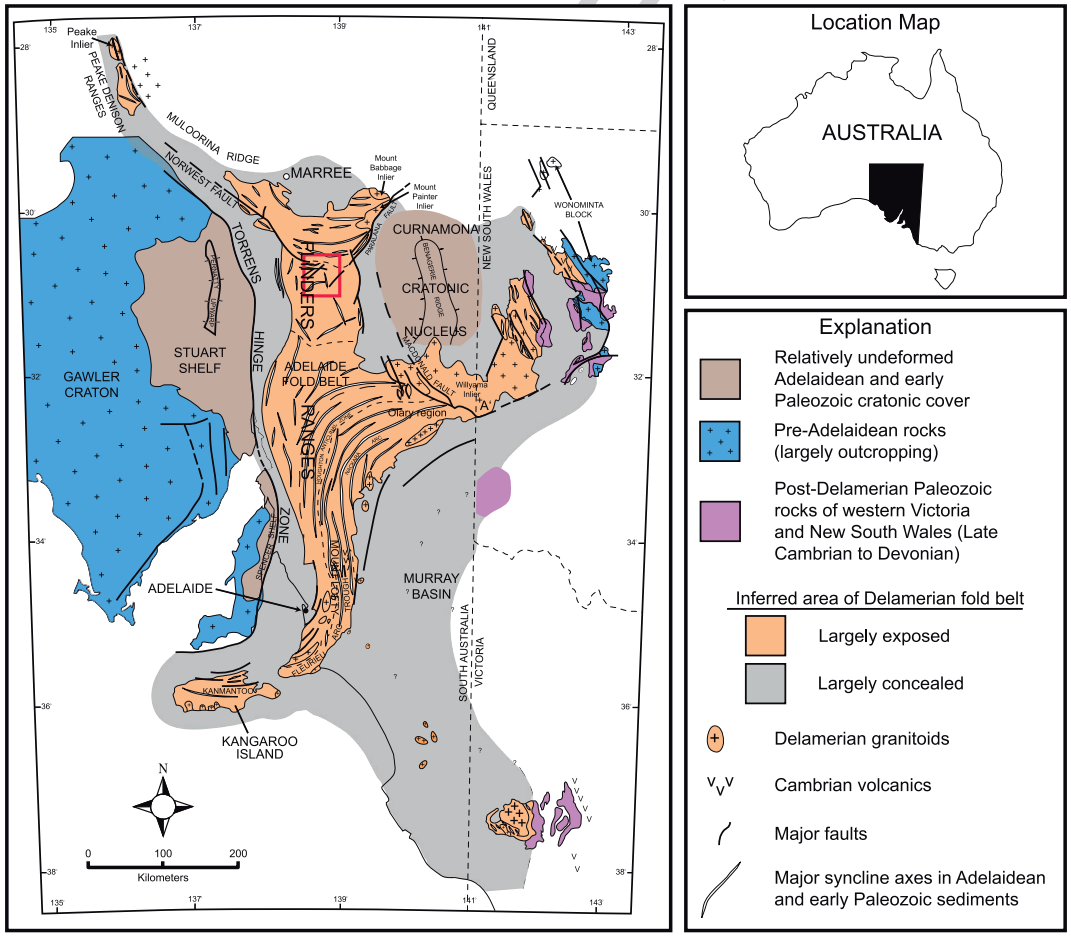

FIGURE 2 Main tectonic provinces and structural domains in eastern South Australia. Red dashed rectangle indicates the location of the studied area. Modified from Hearon, Rowan, Lawton, et al. (2015), originally after Preiss (1987a)

to Ordovician (ca. 500 Ma, Foden et al., 2006; Preiss, 1987a; Sandiford et al., 1998; Paul et al., 2000) or with an earlier onset in the latest Neoproterozoic (Jenkins, 1990; Lemon, 1988, 2000; Rowan et al., 2019; Rowan & Vendeville, 2006; Turner et al., 2009). The Delamerian Orogeny was a major shortening event that impacted the evolution of the structures studied in the present work.

2.1 | Stratigraphy

A detailed review of the stratigraphic record and depositional settings of the Northern Flinders is beyond the scope of our manuscript. The interested reader will find thorough sedimentary and stratigraphic descriptions in publications covering the regional geology of the area: Dalgarno and Johnson (1968), Dalgarno (1998), Preiss (1990, 1993, 2000), Preiss and Cowley (1999), Hearon, Rowan, Giles, et al. (2015). However, a general overview of the stratigraphic record found in Warraweena is offered for completeness (Figure 3).

The oldest exposed rocks comprise the Neoproterozoic Callanna Group (Willouran in age, ca. 850–800 Ma), a typically brecciated mixture of non-marine and marine sedimentary rocks and occasional volcanics (Preiss, 1987a). Where in its correct stratigraphic position, for example in parts of the Willouran Ranges, it comprises a layered sequence of carbonates, fine- to coarse-grained siliciclastics and volcanic rocks that were originally interbedded with evaporites (Preiss, 1987a; Rowan et al., 2019). The most common lithologies are dolostones, dolomitised limestones, sandstones and thinly laminated siltstones. Moulds of halite crystals (known as salt hoppers) and other pseudomorphed evaporite minerals, mm to cm in size and present in sandstones, indicate the former presence of evaporites and are diagnostic of the 5 Callanna Group. The usual appearance of the Callanna rocks in the field is that of breccias and megabreccias discordant with overlying and underlying strata, with chaotic and heavily oxidised cm- to km-scale blocks of Callanna Group lithologies surrounded by a blue-grey carbonate matrix that contains rounded, pebble-sized carbonate clasts (Coats, 1964; Forbes, 1990; Hearon, Rowan, Giles, et al., 2015; Hearon, Rowan, Lawton, et al., 2015; Preiss, 1987a; Preiss, 2000; 6 Webb, 1960). Where remnant bedding is still recognisable, it tends to exhibit large internal shear with recumbent, disharmonic and ptygmatic folding. For simplicity, throughout the manuscript we will refer to these as Callanna breccias. The origin of the Callanna rocks brecciation has been ascribed by some workers to the Delamerian Orogeny (Burns et al., 1977; Mendis, 2002; Mount, 1975), in contrast to many others, who cite evidence for long-lived passive growth of salt diapirs that were later squeezed during the Delamerian Orogeny (Coats, 7 1965; Dalgarno & Johnson, 1968; Dyson, 1996, 1998; Hearon, Rowan, Giles, et al., 2015; Kernen et al., 2012, 2019; Lemon, 1988; Preiss, 1987b; Rowan & Vendeville, 2006; Rowan et al., 2019). Signs of a diapiric origin include composite halokinetic sequences and diapir-derived detritus redeposited in adjacent strata. Thus, the Callanna Group represents one of the earliest records of salt movement and evacuation on Earth. At the surface, it represents a caprock assemblage where halite is no longer present, and gypsum has been altered to the pervasive carbonate matrix (Dalgarno & Johnson, 1968; Dyson, 1996, 1998; Hearon, Rowan, Giles, et al., 2015; Lemon, 1988; Rowan et al., 2019; Webb, 1960).

The overlying Burra Group (Torrensian) comprises the oldest suprasalt rocks in the Adelaide Fold Belt. These units, however, are not exposed in the Warraweena area (Figure 4). The scarce outcrops nearby are restricted to a few square kilometres of dolomitic siltstones, shales and quartzites of the Copley Formation lying along the hinge of the Mount Morris Anticline north of Warraweena Station (Figures 4 and 5), beyond the limits of our studied area. The predominant lithologies are quartzites, dolomites and finely grained siliciclastics (mostly shale and siltstone). Although the exposed thickness is less than 550 m, the entire Burra Group is interpreted to be up to 3-km thick at depth in the area (Figure 5).

Regionally the Burra Group is overlain by the Umberatana Group, which is Sturtian to Marinoan and comprises: (a) tillites of the Merinjina Formation; (b) marine and non-marine fine-grained, thinly laminated to massive siltstones and shales of the Tindelpina and Tapley Hill formations; (c) algal, oolitic limestones and dolomites of the Balcanoona Formation and (d) arkosic, medium-grained, cross-laminated sandstones, siltstones and sandy red dropstones with minor beds of diamictites of the Elatina Formation. The thickness of the exposed Umberatana Group reaches up to ca. 1,500 m on the southern flank of the Mount Goddard Syncline (Figures 4 and 6), although it is not exposed all around the studied area. The thickness is interpreted to increase dramatically towards the cores of the Mount Morris (where the Burra is exposed) and Mount Stuart anticlines, reaching more than 5 km (Figure 5).

The youngest sequence of Neoproterozoic rocks is the Wilpena Group (Marinoan to Ediacaran), which is characterised by an upward-shallowing succession of shelfal, fine-grained siliciclastics and carbonates, along with shoreface sandstone and peritidal carbonates (Preiss, 1987a, 2000). The oldest units in the Wilpena Group comprise strata deposited during worldwide glaciation (Preiss, 1987; Preiss et al., 2011). The youngest units contain fossils of the Ediacaran fauna (Hearon, Rowan, Giles, et al., 2015; Preiss, 2000). The Wilpena thickness in the field area is in the range of 4–5 km, but dramatically increases to nearly 7.5 km towards the centre of the synclines neighbouring the Warraweena diapir-weld-thrust system (Figures 4 and 5). From older to younger, the Wilpena Group consists of: (a) the Nuccaleena Formation, composed of thinly laminated micritic dolomites with interbedded shales at the top; (b) red and olive-green siltstones, shales and sandstones of the Brachina

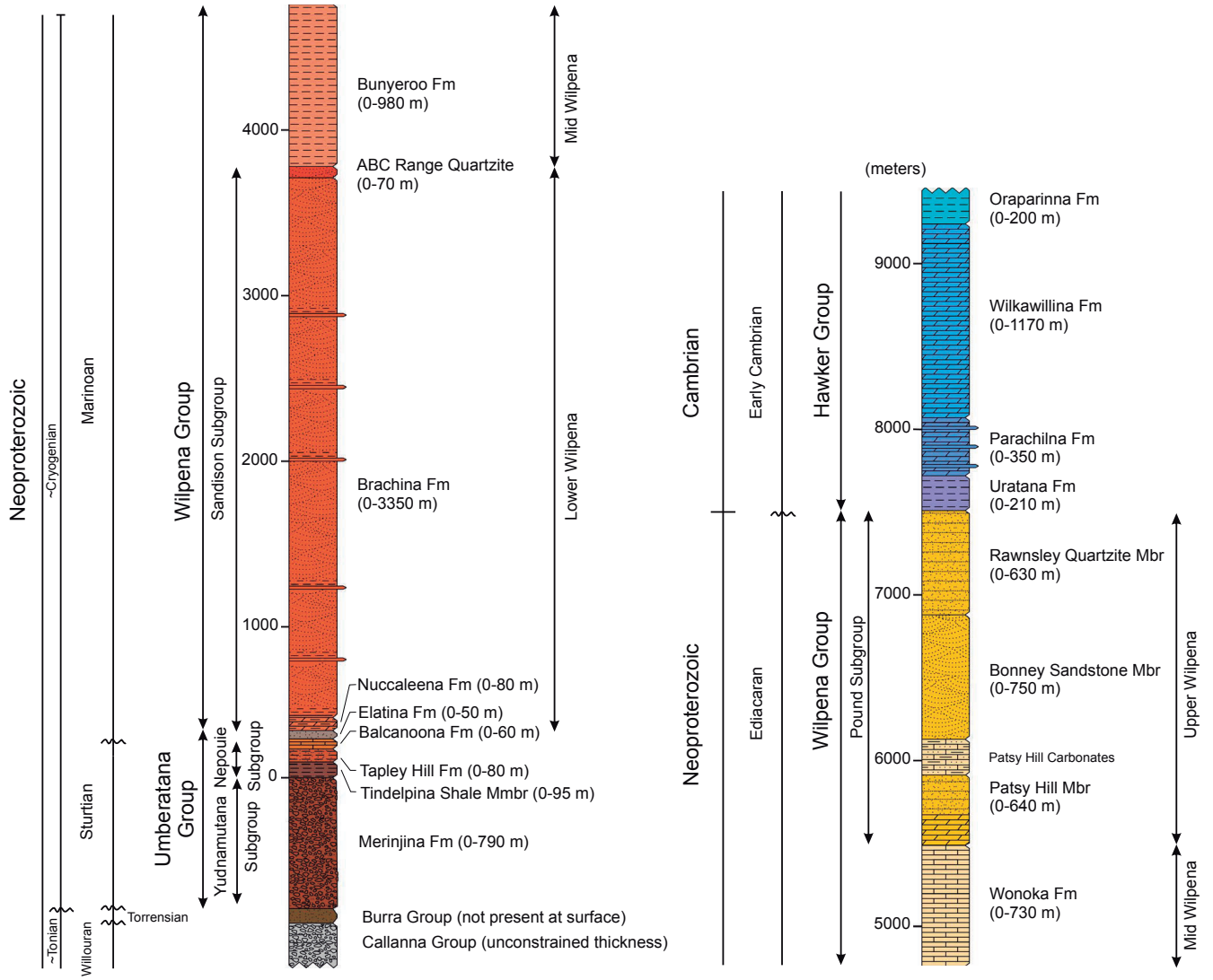

FIGURE 3 Stratigraphy of the Neoproterozoic and Cambrian units outcropping in the Warraweena area. Thicknesses are average values observed within the mapped area

Formation; (c) pinkish-grey cross-bedded and rippled quartz arenites of the ABC Range Quartzite; (d) grey-red to grey-green fine-grained sandstones, siltstones and shales of the Bunyeroo Formation; (e) grey calcareous shales, dolomites, limestones and siltstones of the Wonoka Formation and (f) the Pound Subgroup, largely composed of sandstones, quartzites and siltstones, and subdivided into three members (the thinly laminated green shales, cherty dolomites and dark-yellow quartz arenites of the Patsy Hill Member, the reddish-brown to yellowish quartz arenites of the Bonney Sandstone Member and the cross-bedded and rippled subarkose to quartz arenite and quartzite of the Rawnsley Quartzite Member, which contains the Ediacaran Fauna).

Overlying the Wilpena Group are Lower Cambrian strata of the Hawker Group, which comprise turbiditic and stromatolitic reefal limestone units with minor interbedded clastics. More specifically, four units are described in the studied area: (a) the olive-green micaceous shales, orthoquartzites and grey cross-bedded sandstone with limestone nodules of the Uratanna Formation; (b) the rippled argillaceous sandstones, shales and lenticular limestones of the Parachilna Formation; (c) the grey biostromal, brachiopod-bearing and stromatolitic limestones of the Wilkawillina Formation and (d) the green, finely micaceous carbonaceous siltstones of the Oraparinna Shale. The preserved thickness of the Hawker Group in the Warraweena area is up to ca. 2 km in the centres of the synclines (Figure 5).

2.2 | Structural framework

The structural features of the Warraweena area are described in more detail in later sections of the manuscript. However, a general description of the regional structural style will help to put later local observations and descriptions in context.

The structural style of the region is characterised by multiple structural trends (see Figure 4). Although broad,

COLOUR online, B&W in print

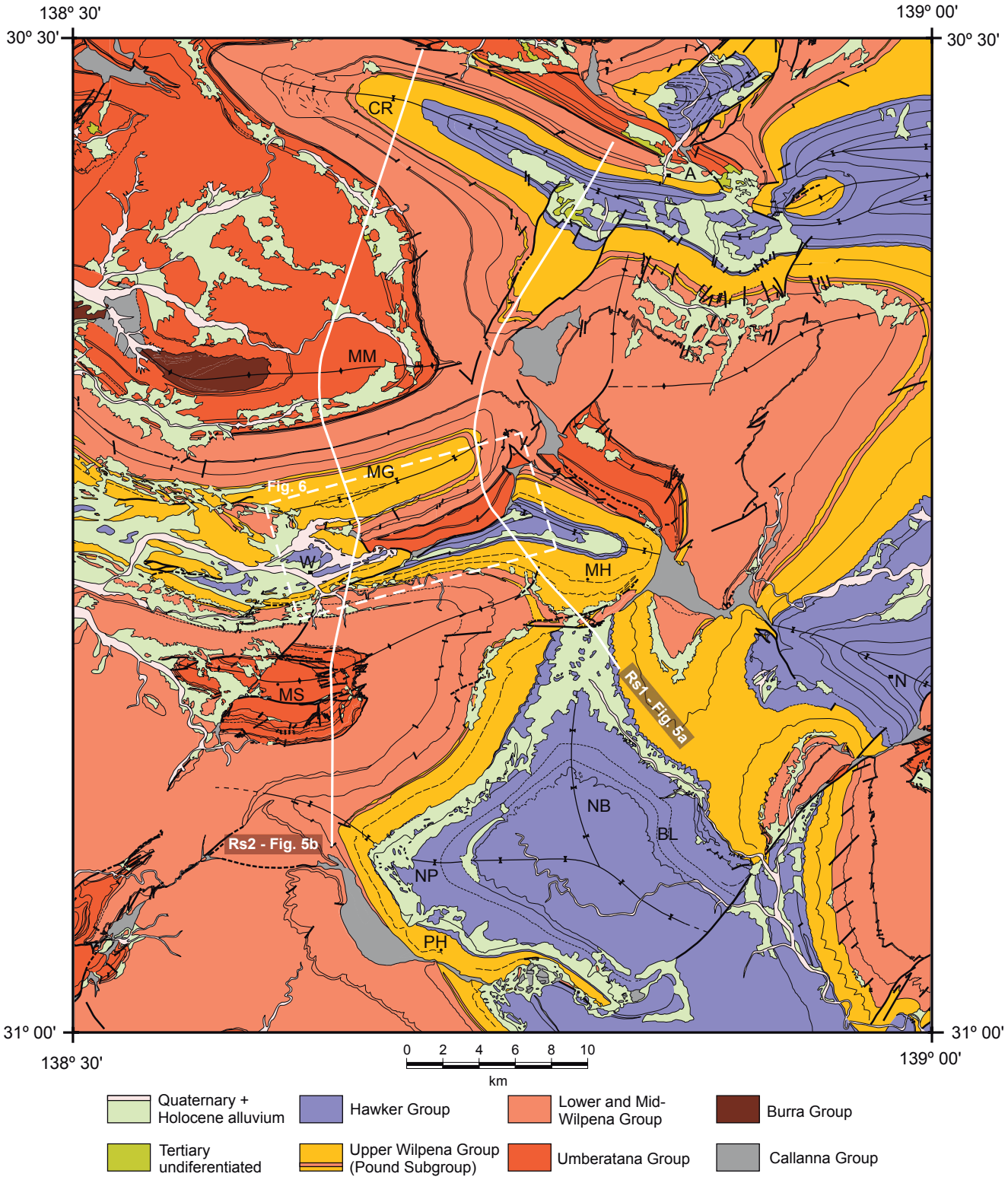

FIGURE 4 Simplified geological map of the portion of the Flinders Ranges containing the study area. Map has been simplified and modified after Coats (2009). Dashed white rectangle indicates the location of the Warraweena area mapped in detail in this work. The two solid white lines indicate the location of the regional sections shown in Figure 5. A, Angepena Station; BL, Ben Lomond; CR, Castle Rock; MG, Mount Goddard; MH, Mount Hack; MM, Mount Morris; MS, Mount Stuart; N, Nantawarrina; NB, Narrina Basin; NP, Narrina Pound; PH, Patawarta Hill; W, Warraweena Station. The thin orange section near the base of the Pound Subgroup is the carbonate facies within the Patsy Hill Member

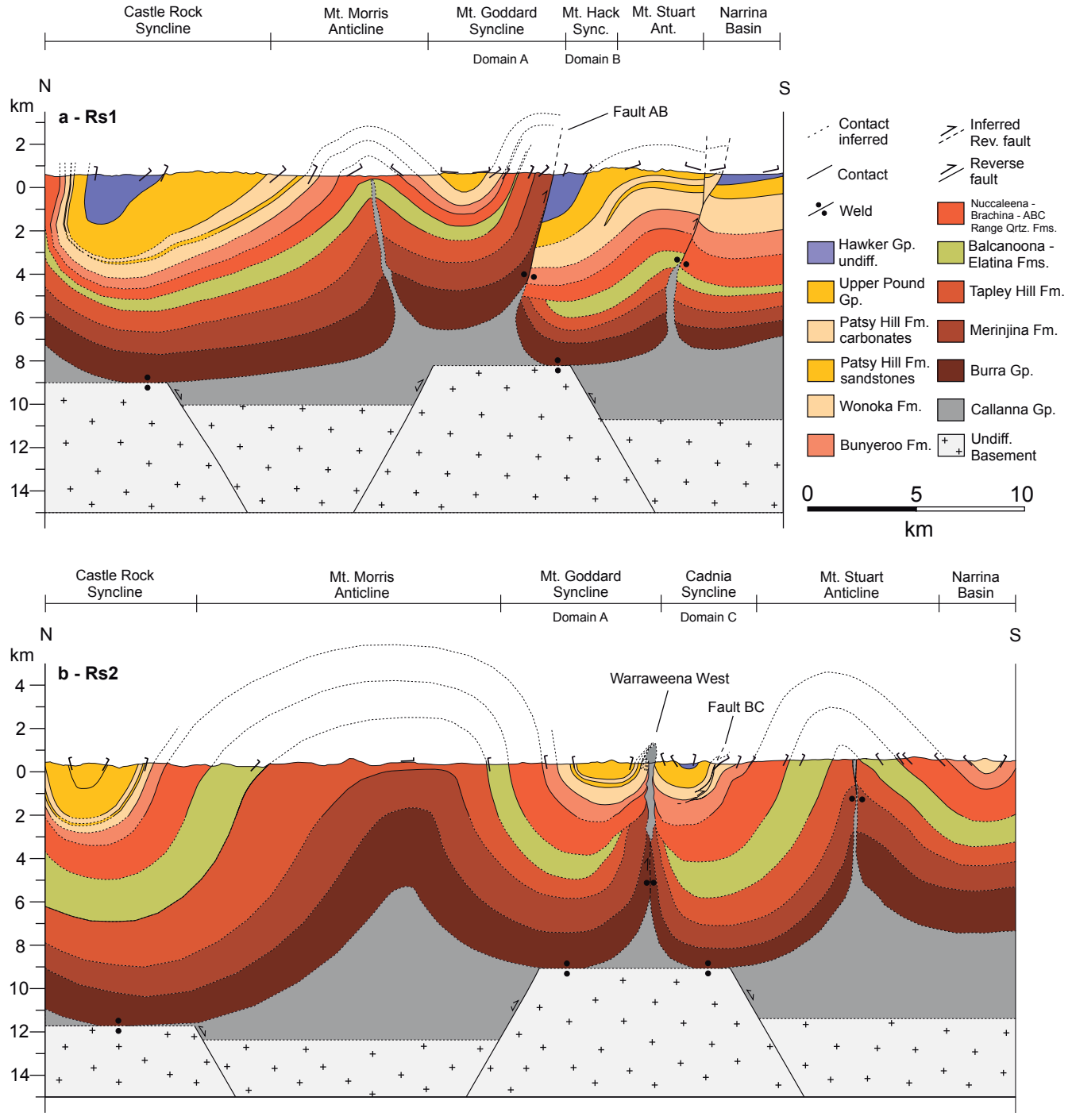

FIGURE 5 Regional cross sections across the area constructed with collected field data and available geological maps (Coats, 1973, 2009). Dashed lines indicate inferred interpretation in the unconstrained subsurface. See Figure 4 for location

long-wavelength anticlines, synclines and apparent thrust faults generally trend WNW-ESE to WSW-ENE, there are also structures with more N-S trends. Bodies of Callanna breccia also have variable trends and are usually located along the hinges of anticlines or along fault systems. The complexity of the large-scale geometry is interpreted to reflect some combination of inversion of the precursor rift architecture and shortening of pre-existing diapirs and minibasins (Backé et al., 2010; Rowan & Vendeville, 2006). The different structural trends and the complexity added by the presence of pre-existing diapiric bodies makes is difficult to determine the main orientation of the Delamerian shortening. We infer that NNW-SSE directed shortening affected the pre-existing structures, based on large-scale fold orientations seen on maps (Figure 4). However, a component of vertical-axis rotation cannot be ruled out (Rowan & Vendeville, 2006).

COLOUR online, B&W in print

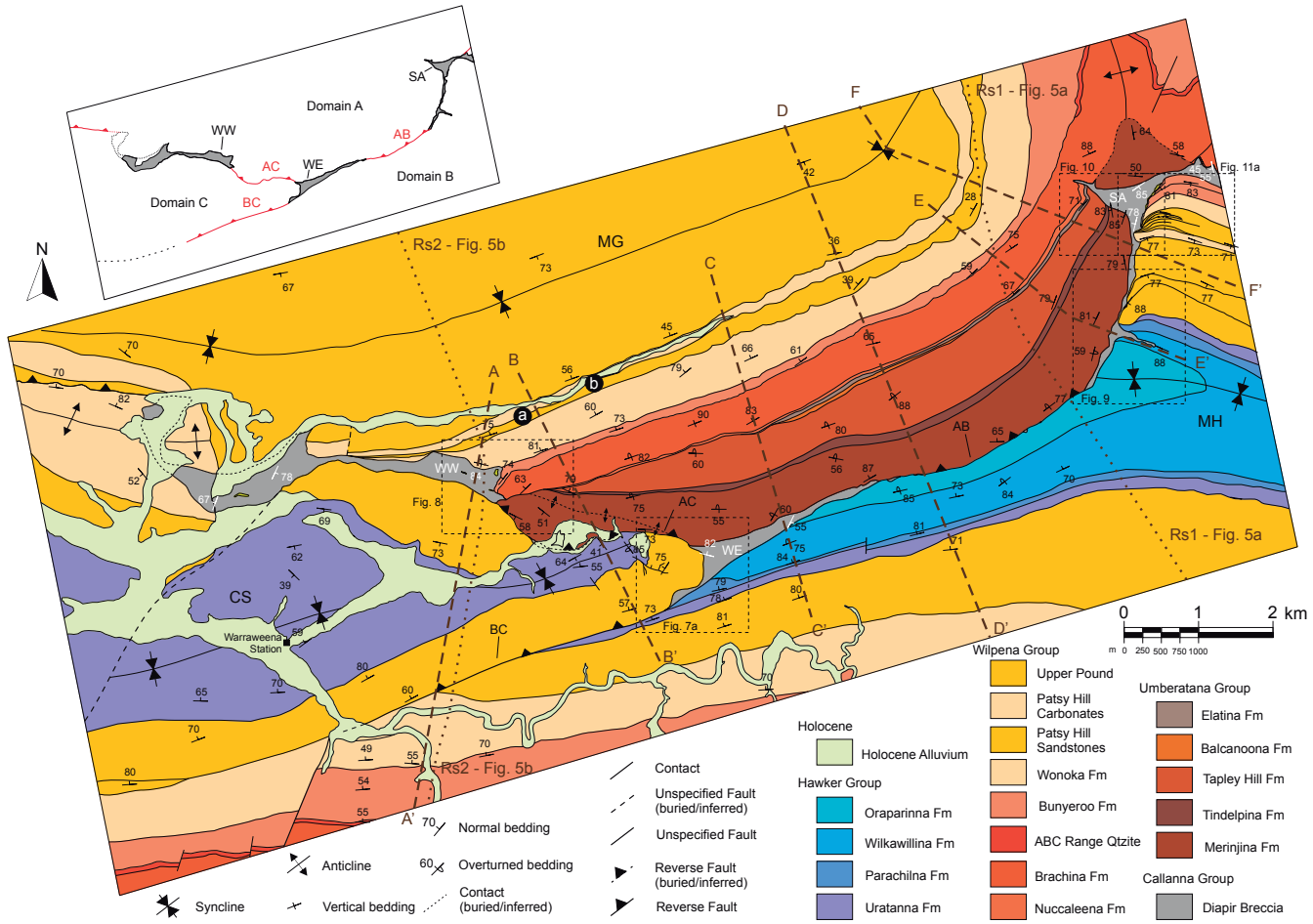

FIGURE 6 Geological map of the Warraweena area. See Figure 4 for location. Dotted lines Rs1 and Rs2 indicate, respectively, the trace of regional sections in Figure 5a,b within the studied area. Dashed lines A to F indicate location of cross sections in Figure 12. Labels refer to key structures described in the text. CS, Cadnia Syncline; MG, Mount Goddard Syncline; MH, Mount Hack Syncline; WW, Warraweena West Diapir; WE, Warraweena East Diapir; SA, South Angepena Diapir; AC, Fault Segment AC; AB, Fault Segment AB; BC, Fault Segment BC. Labels a and b inside the black circles indicate approximate location of photos shown in Figure 13a,b respectively. Inset map at the top left displays the structural domains and linking structures cited in the text

The subsurface geometry is largely unknown. In general, the anticlines are interpreted to be cored by rocks of the Callanna Group (Figure 5) based on analogous structures throughout the Flinders Ranges. Evaluation of published regional maps suggests that the anticlines originated as asymmetric synclinal depocentres (as indicated by the large thickness differences between flanks, particularly in the Mount Morris Anticline and, to a lesser degree, the Mount Stuart Anticline, Figure 4), later inverted during the Delamerian Orogeny. This is also supported by the thickening of the Umberatana Group units (i.e. from the Merinjina to the Elatina Fms.) towards the anticlinal hinges. The presalt structure is thus postulated to be a set of partially inverted basement-involved extensional faults (Figure 5). These would have controlled an early morphology where Neoproterozoic minibasins were located above the rift hanging walls, whereas inflated salt and thinned strata developed over the footwalls (similar to experimental models by Warsitzka et al., 2015). During the Delamerian Orogeny, partial inversion of the basement faults and possible footwall buttressing would have led to salt inflation above the rift hanging walls, formation of Callanna-cored anticlines and thrust faults and squeezing of any pre-existing diapirs. This geometry is exposed in the plunging Yankaninna anticline and the Mt. Painter inlier basement inversion structure northeast of the study area (J. A. Muñoz, pers. comm., 2019; 1:250,000 Copley sheet, Coats, 1973).

3 | STRUCTURAL DESCRIPTIONS OF THE WARRAWEENA AREA

The deformation and structural styles in the Warraweena area are described at three different scales. First, the regional to macro-scale (i.e. km-scale) structure is summarised based on field observations and the base maps available in the area (scale 1:100,000 by Coats, 2009 and scale 1:250,000 by

Coats, 1973) as well as satellite images (confidential, courtesy of ConocoPhillips). The field observations include mapping and geometrical relationships of the principal folds, faults and breccia bodies. Second, meso-scale (i.e. metres to hundreds of metres) structures in the area are characterised based on detailed mapping and construction of structural transects across key domains. These include smaller faults and folds as well as tectono-sedimentary relationships and salt-sediment interface features (e.g. halokinetic sequences, local debris flows and caprock). Finally, small-scale (i.e. mm to cm) structures (principally fractures and cleavage) are described and evaluated.

The study area is divided into three structural domains (Figures 5 and 6): the WSW-ENE trending Mount Goddard Syncline (Domain A) in the north; the NW-SE Mount Hack Syncline (Domain B) in the southeast and the WSW-ENE Cadnia Syncline (Domain C) in the west. The three domains are separated from each other by a complex system of Callanna brecciated bodies and faults. The system displays an overall arcuate structural trend that varies from E-W in the west (in the vicinity of Warraweena Station) to N-S in the eastern termination (just south of Mucatoona Hill; Figures 4 and 6). Below, we describe first the dividing system of breccias and faults and then the details of the three structural domains.

3.1 | Dividing structures

The dividing structures comprise three different Callanna-brecciated bodies and their connecting or branching fault segments. At a triple junction of three segments is the WSW-ENE oriented Warraweena East (WE) breccia (Figure 6, map and inset). The Warraweena East structure is nearly 3.2-km long, with a width ranging from 0 to ca. 450 m. Because it is the only breccia body between each pair of structural domains, it has a forked geometry with three terminations: the northwestern prong separates Domains A and C; the southwestern tip divides Domains C and B and the main body extending to the east is in between Domains A and B. The three terminations of Warraweena East thin rapidly, transitioning to apparent faults with the northern domains upthrown: fault AB separates Domains A and B, fault AC separates Domains A and C and fault BC separates Domains B and C (Figure 6).

The northwestern end of Warraweena East is a good example of the transition from the Callanna breccias to apparent faults (Figure 7a). The tip is a highly deformed area of Callanna breccia, about 15-m thick, in contact with a highly altered and oxidised sequence of tillites of the Merinjina Formation (Figure 7b). Some dozens of metres further to the northwest, no trace of Callanna breccia is found, and the Merinjina Formation in Domain A is juxtaposed against the Rawnsley Formation (Pound Subgroup) in Domain C along fault AC. This arcuate fault is 3-km long, and displays no Callanna breccia until it links to the Warraweena West structure to the northwest (Figure 6).

The southwestern termination of Warraweena East (Figures 6 and 7) contains patchy Callanna breccia outcrops, tens of metres in size, that separate the Rawnsley Formation (mapped as part of the Pound Group) in Domain C (northwestern side) from the carbonate sequences of the Uratanna and Parachilna formations in Domain B (southeastern side). This transitions to an apparent linear thrust fault (fault BC) that dies out to the WSW. The northeastern prong of the Warraweena East structure thins out progressively, merging with the roughly 2.8-km-long fault AB that links to the South Angepena structure (SA; Figure 6).

The ca. 5-km long, roughly E-W oriented, Warraweena West (WW) structure is an outcrop of Callanna breccias, 0- to 500-m wide, separating Domain A to the north from Domain C to the south. Fault AC intersects the breccia body at a corner, and the southern edge of the breccia is relatively smooth, whereas the eastern and northern sides of Warraweena West are characterised by abrupt trend changes (Figures 6 and 8). To the west, Holocene alluvium partly covers the bedrock, but the breccia is interpreted to curve to the north, where it connects to an E-W trending thrust fault extending out of the study area to the west (Figure 6).

The South Angepena (SA) breccia body exhibits an overall SSW-NNE orientation, is nearly 4 km in length and has significant variations in width up to nearly 1.1 km. It separates Domains A and B and has several prongs extending into these domains (Figures 6 and 9–11). The main body of Callanna breccia to the south is ca. 50- to 100-m wide on average and occasionally thins to ca. 25–35 m. An E-W trending strip of Callanna breccia extends out into the Cambrian stratigraphy of Domain B (Figure 9). The strip is ca. 530 m long and displays a width ranging from 200 m in the west, to 25 m in the centre and 45 m in the east. To the north, the Callanna breccia expands into a triangular body that narrows to the northwest into Domain A (Figure 10). Farther north, the Callanna breccia is folded to trend roughly E-W and thins to the east, eventually dying out near the vicinity of the Old Angepena Station, beyond the limits of the studied area. In this area, a ca. 25-m-wide strip of rock with a pervasive but discontinuous, elongated fabric (informally called *chips*) is observed within, but at the margin of the Callanna breccia (Figure 11b). The chips are mm to cm in size, comprise silicified dolomite, and are roughly aligned in the fashion of a pseudo-foliation. Although less well preserved, a similar fabric is also observed further south within the outermost Callanna breccia. This texture is characteristic of the southeastern boundary of the South Angepena structure, but it is not observed at the margins of other Callanna breccia bodies.

3.2 | Domain A: The Mount Goddard Syncline

The Mount Goddard Syncline is a ca. 17-km long and 8.5-km wide, arcuate syncline trending E-W to ENE-WSW.

COLOUR online, B&W in print

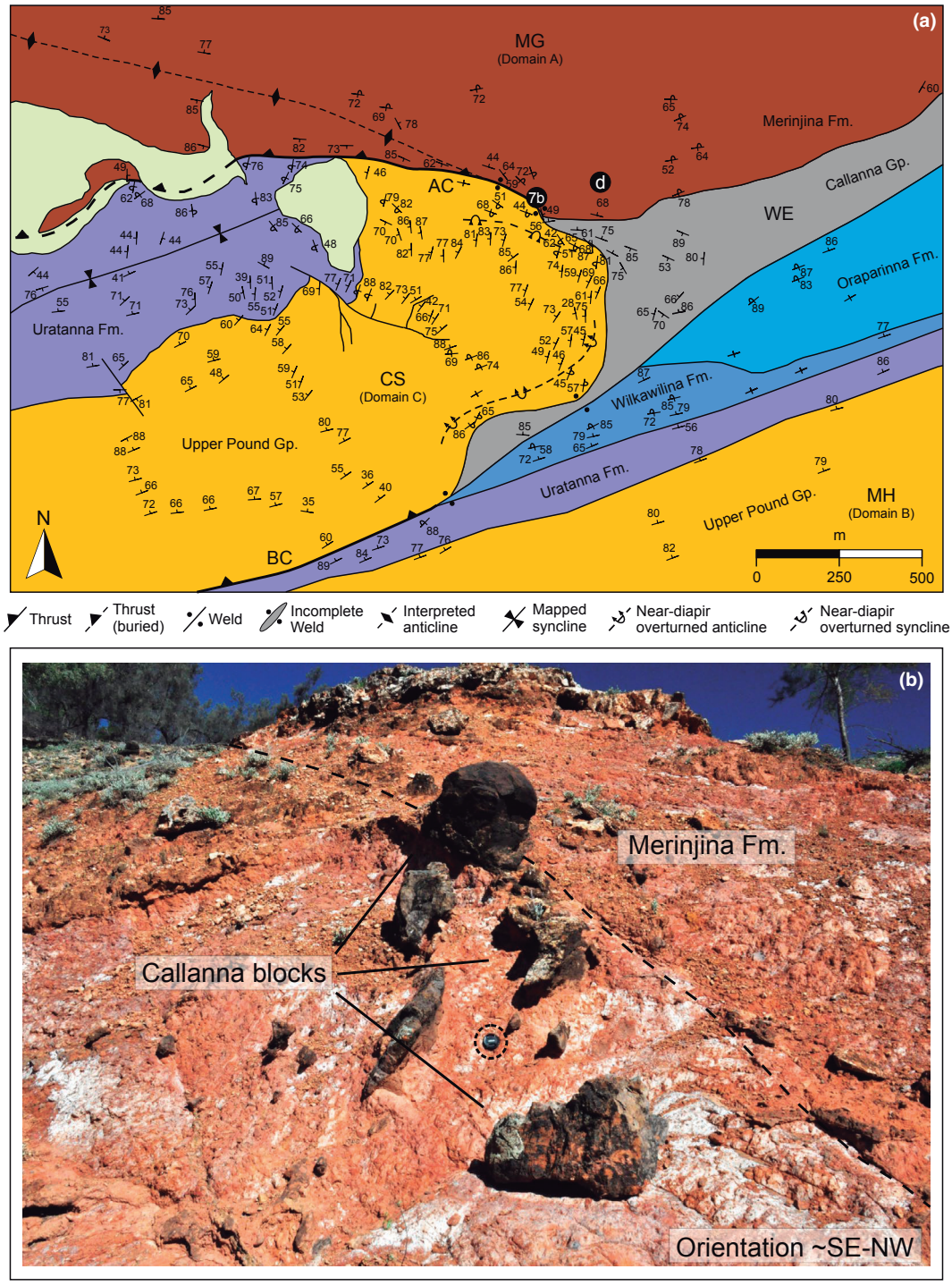

FIGURE 7 (a) Geological map of the Warraweena East diapir (WE) showing the relationship between the Mount Goddard (MG), Cadnia (CS) and Mount Hack (MH) minibasins across fault segments AC and BC, respectively, and across the diapir. Colour legend and labels are the same as in Figure 6. Label d inside the black circle indicate approximate location of photo shown in Figure 13d. (b) Field photo taken at the NW tip of WE, near fault segment AC, showing highly deformed and altered Merinjina Fm. in contact with the Callanna breccia blocks (dark area of Callanna, around 15-m thick; see label 7b on the map above for location). Photograph looks towards the SSW. Black dotted circle highlights lens cap for scale. See Figure 6 for the location of this map in the subregional context

The exposed stratigraphy displays a maximum thickness of ca. 4.2 km in the central sector of the southern limb. The strata here comprise the Umberatana and Wilpena groups, separated by a ca. 10-km-long unconformity at the base of the Nuccaleena Fm. (Figure 6). Below the unconformity, the Umberatana Group thins laterally towards both the Warraweena West and South Angepena Callanna breccia bodies. Above, the Wilpena is generally tabular, with minor thickness variations accentuated near the Callanna breccia bodies. Dips range from moderate near the synclinal hinge to

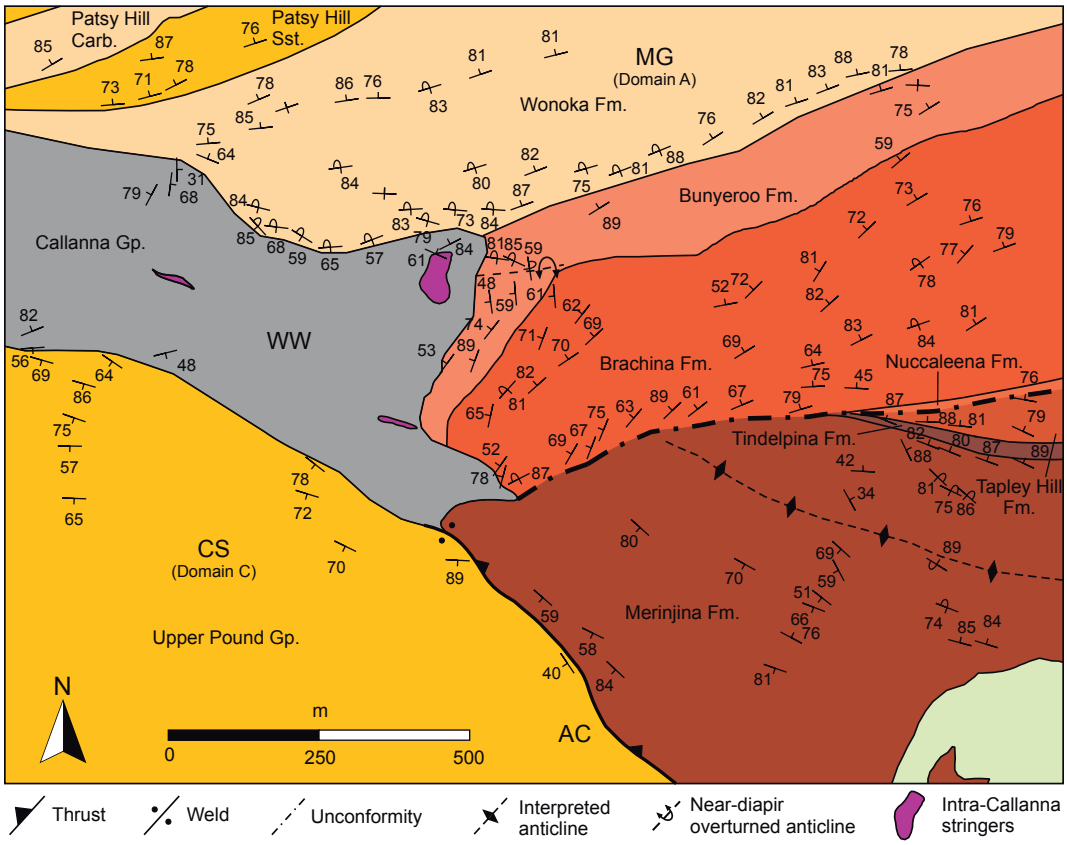

FIGURE 8 Geological map of the eastern portion of Warraweena West diapir (WW) showing the general features and meso-scale deformation described in this sector between the Mount Goddard (MG) and the Cadnia (CS) synclines. Notice the different structural styles in the in the Wilpena Group of the Mount Goddard Syncline near the salt and near fault segment AC. Colour legend and labels as in Figure 6. Some intra-Callanna stringers indicated in purple. See Figure 6 for the location of this map in the subregional context

overturned closer to the bounding faults AB and AC and the associated breccia bodies.

In the vicinity of Warraweena West (Figure 8), the Umberatana Group is restricted to a NW-thinning sequence of the Merinjina Fm. Strata are generally steep, between 60º and 90º away from the breccia and often slightly overturned. The base-Wilpena unconformity, separating the base of the Nuccaleena Fm. from the underlying units, intersects the Callanna breccia at a prominent cusp in its edge. The bedding of the overlying Brachina and Bunyeroo fms. displays a general WSW-ENE trend that folds down towards the Callanna breccia, leading to tight, overturned folds of tens of metres in size. The contact between the Bunyeroo and Wonoka fms. intersects the breccia at another, larger cusp, with bedding in the lower Wonoka Fm. displaying a steady SSW-NNE trend and near-vertical dips until within ca. 30–50 m of the Callanna breccia, where the Wonoka beds become more overturned and strike parallel to the edge of the breccia (Figure 12a). Continuing upward, the upper Wonoka Fm. and Pound Gp. thin towards the northern interface of Warraweena West in an apparent onlap relationship (Figure 12a).

To the east and southeast of Warraweena West (Figures 6 and 8), the bedding of the Umberatana Group is broadly parallel to the southern boundary of Domain A and is steeper (near vertical to overturned) than the Wilpena Group, highlighting the presence of the previously mentioned base-Wilpena unconformity (i.e. base of the Nuccaleena Fm; Figure 12b). Another minor unconformity is defined by the contact between the Tindelpina and the Merinjina fms. with the Brachina Fm. as beds generally steepen closer to the Callanna breccias and fault segments (Figure 12a–d). However, there is a notable difference depending on position: whereas progressive steepening towards the Callanna breccia characterises the breccia-flanking strata (Figures 8 and 12a,c), those along the intervening fault segments first steepen but then become gentler, forming minor anticlines juxtaposed against the faults (Figure 12b,d).

The southern limb of the Mount Goddard Syncline gradually becomes less steep near the South Angepena structure (Figures 6 and 9). Locally, however, NW-ward dipping beds steepen towards the bounding fault or breccia: 75º–80º in the Merinjina Fm., ca. 65º in the Elatina Fm. and 45º–35º in the Wilpena Group (Figure 12e,f). The NW-SE trending edge of South Angepena truncates the bedding from the base of the Umberatana Group all the way up to the base of the Brachina

COLOUR online, B&W in print

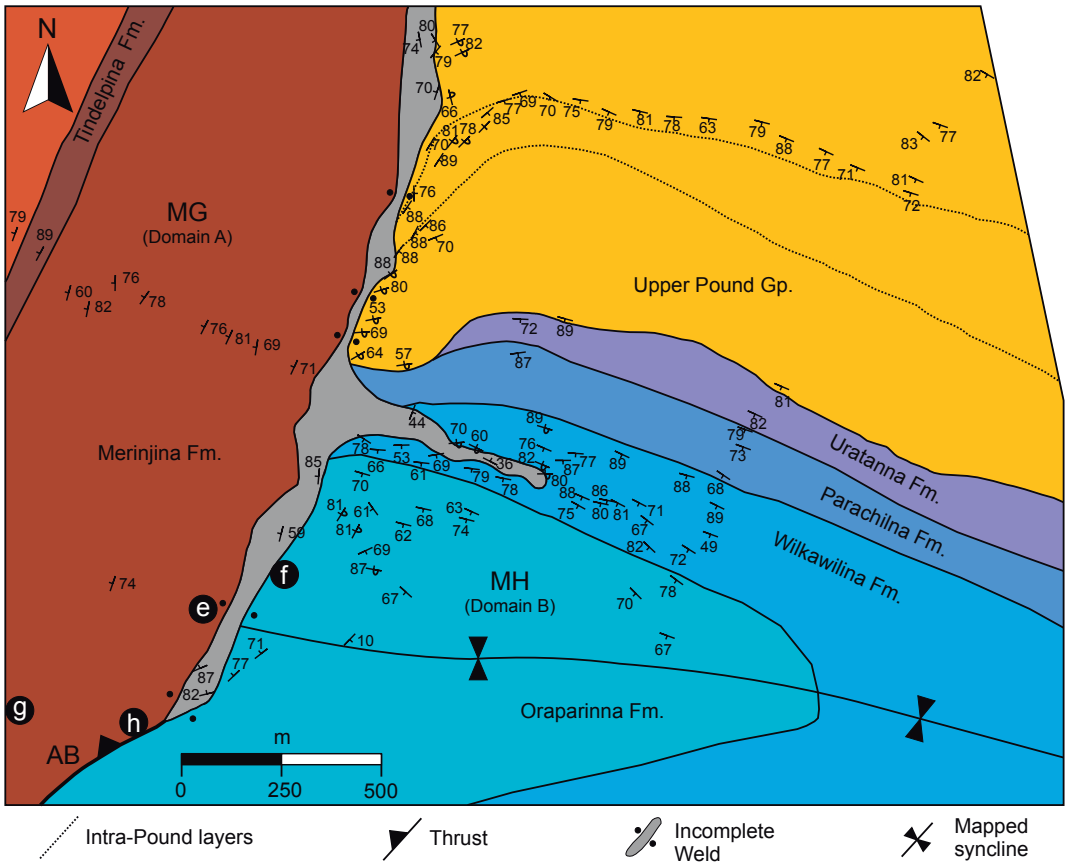

FIGURE 9 Geological map of the area just south of the South Angepena diapir (SA). Notice the presence of the salt wing extending out into the Cambrian sediments of the Hawker Group. North of the salt wing bedding of the Pound Subgroup strikes roughly WNW-ESE up to the last few hundreds of metres away from the salt, where it gradually rotates to a N-S to NNE-SSW strike, often overturned. Labels e, f, g and h inside the black circles indicate approximate locations of photos shown in Figure 13e–h respectively. Colour legend and labels as in Figure 6. See Figure 6 for the location of this map in the subregional context

Fm. in the Wilpena Group (Figure 10). Within 200 m of South Angepena, bedding becomes steeper and subparallel to the Callanna breccia interface before forming an overturned anticline of ca. 100 m in wavelength, predominately in the Tapley Hill Fm (Figure 10).

Small-scale deformation varies throughout Domain A. Away from the breccia-fault systems, metre-scale thrusts and folds are occasionally observed (Figure 13a), as are swarms of fractures that include bedding-parallel, cross-strike and strike-oblique orientations (Figure 13b). Starting in the west and moving along the southern edge of the domain, the Warraweena West area is characterised by metre-scale, tight, overturned folds developed within 30 m of the Callanna breccia interface, particularly in the Bunyeroo, Wonoka and Pound stratigraphic sequence. The Merinjina Fm. adjacent to fault AC locally displays a minor shear fabric, metre-scale ca. E-W trending folds and NW-SE trending fractures dipping 70°–85° mostly to the NE. Near the Warraweena East structure, two main fracture sets are well expressed: a moderately dipping (30°–60°) NW-SE set and a subvertical NE-SW set (Figure 13d). Other than this, deformation is not qualitatively different than farther away from the breccia. Fault AB is associated with several tight folds (Figure 13g), an increased presence of NE-SW trending fractures, a fault-parallel cleavage (roughly E-W) and a 1- to 3-m wide shear zone along the fault (Figure 13h). Finally, near the South Angepena breccia small-scale asymmetric folds and thrusts are observed (Figure 13e) that become somewhat more common where the Callanna breccia is <50-m wide. Many breccia-flanking areas are, however, effectively undeformed (Figure 13c).

3.3 | Domain B: The Mount Hack Syncline

The Mount Hack Syncline is a ca. 9-km long, WNW-ESE trending structure whose hinge intersects the South Angepena breccia near where it merges into fault AB (Figures 6 and 9). The exposed strata span the upper Wilpena Group to the Cambrian Hawker Group (Figure 12c–f). The northern limb dips consistently 75°–80° towards the SSW (Figures 9 and 11). The southern limb is more variable in orientation, curving from WNW-ESE to ENE-WSW south of Warraweena East and faults AB and BC, where it dips steeply towards

COLOUR online, B&W in print

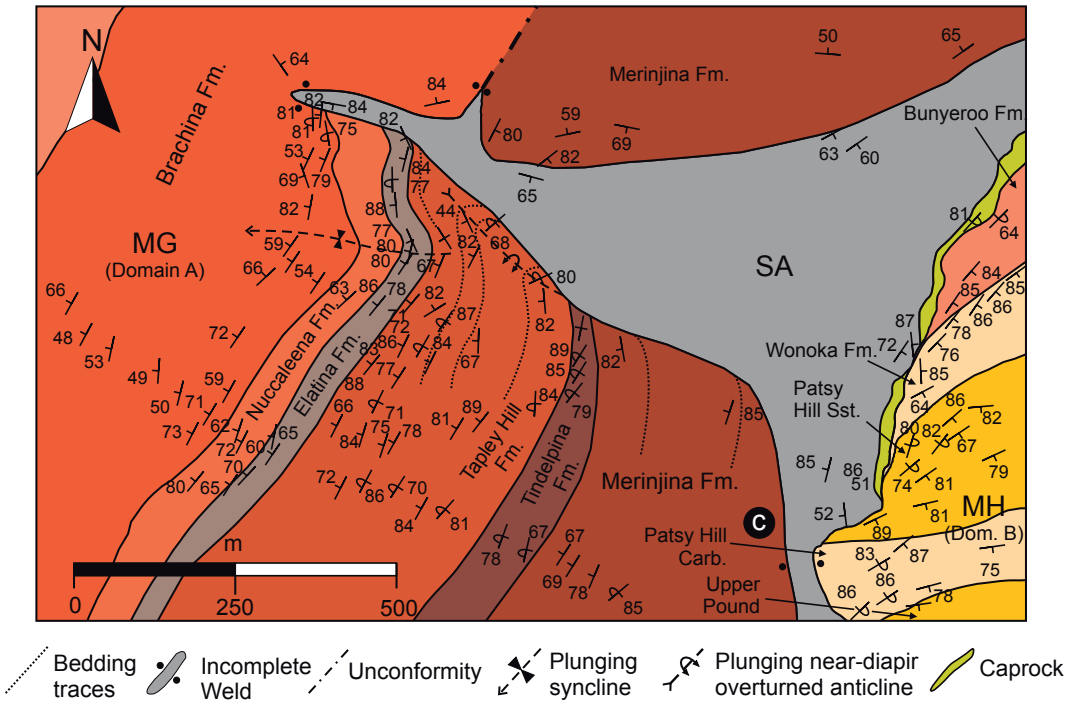

FIGURE 10 Geological map of the SW flank of the South Angepena diapir (SA) and the overlying sequence in the Mount Goddard minibasin (MG). Meso-scale folding takes place mostly just tens of metres away from the salt-sediment interface and is characterised by overturned bedding outlining a tight fold. Colour legend and labels as in Figure 6. Notice the presence of caprock along the eastern salt-sediment interface. Label c inside the black circle indicates the approximate location of photo shown in Figure 13c. See Figure 6 for the location of this map in the subregional context

the breccia-fault system and becomes overturned (Figures 7a and 12c,d).

Strata in the northern limb of the syncline thin and curve within 300 m of the South Angepena structure, steepening slightly and becoming overturned before truncating against the Callanna breccia or becoming parallel to its edge (Figures 9–11). The Bunyeroo to Cambrian section here contains multiple unconformities within 400–800 m of the Callanna breccia interface. The youngest of these is at the base of the thin body of breccia extending out into the northern limb of the syncline within the Wilkawillina Fm (Figure 9), whereas the other unconformities are at the bases of 20- to 50-m-thick conglomerates that thin progressively towards the east, away from the South Angepena structure. These are highly altered adjacent to the breccia and comprise poorly sorted, angular, gravel-sized clasts in a highly weathered and poorly indurated matrix. Some of the underlying unconformities intersect the Callanna breccia with minor changes in the orientation of its boundary (Figure 11a).

Other conglomerates within the northern limb of the Mount Hack Syncline are not associated with unconformities or the South Angepena structure. These conglomerates are gravel to cobble sized, poorly to medium sorted, angular, clast-supported and unaltered. They thin to the west and east, defining channel-like morphologies that suggest a sediment provenance from out of the plane of the surface exposure.

The small-scale deformation in the Mount Hack Syncline is not appreciably different from that in Domain A. It includes fractures (bedding-parallel, cross-strike and strike-oblique), with no systematic increase towards the breccia-fault system, as well as mm- to cm-scale folds in the Cambrian carbonates (Figure 13f). Whether the latter are due to tectonic or soft-sediment deformation is uncertain. Near fault AB there is an increased development of a fault-parallel foliation.

3.4 | Domain C: The Cadnia Syncline

The Cadnia Syncline is located in the west of the studied area. It is an ca. 8-km long, WSW-ENE trending structure bounded by the Warraweena West breccia and fault AC to the north (Figure 12a,b) and fault BC to the south (Figure 12b), with its eastern tip intersecting the Warraweena East structure (Figures 6 and 7). Exposed strata include the upper Wilpena Group and the lower Hawker Group, which dip steeply on both limbs but which reduce in dip towards the fold hinge (Figure 12a,b).

In the eastern sector of Domain C, the structure becomes more complex (Figure 7a). First, beds are vertical to overturned in the northern limb close to fault AC. Second, there are several minor faults in the southern limb. Third, near the north-western tip of the Warraweena East structure,

COLOUR online, B&W in print

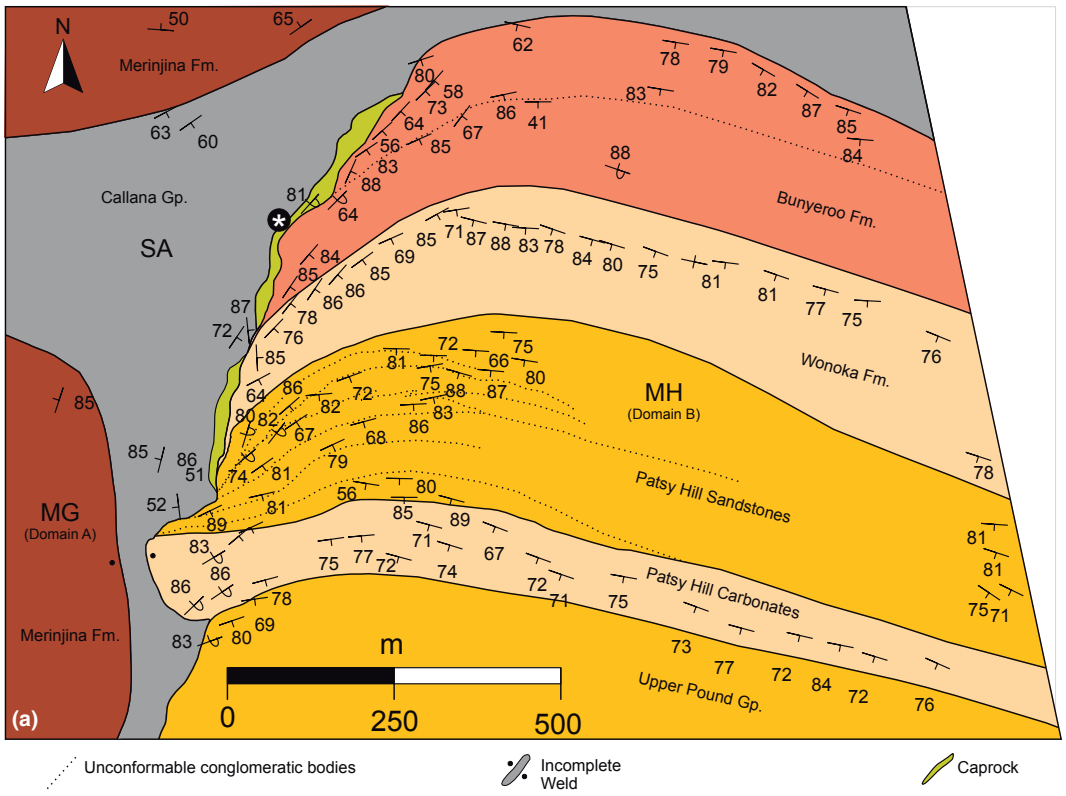

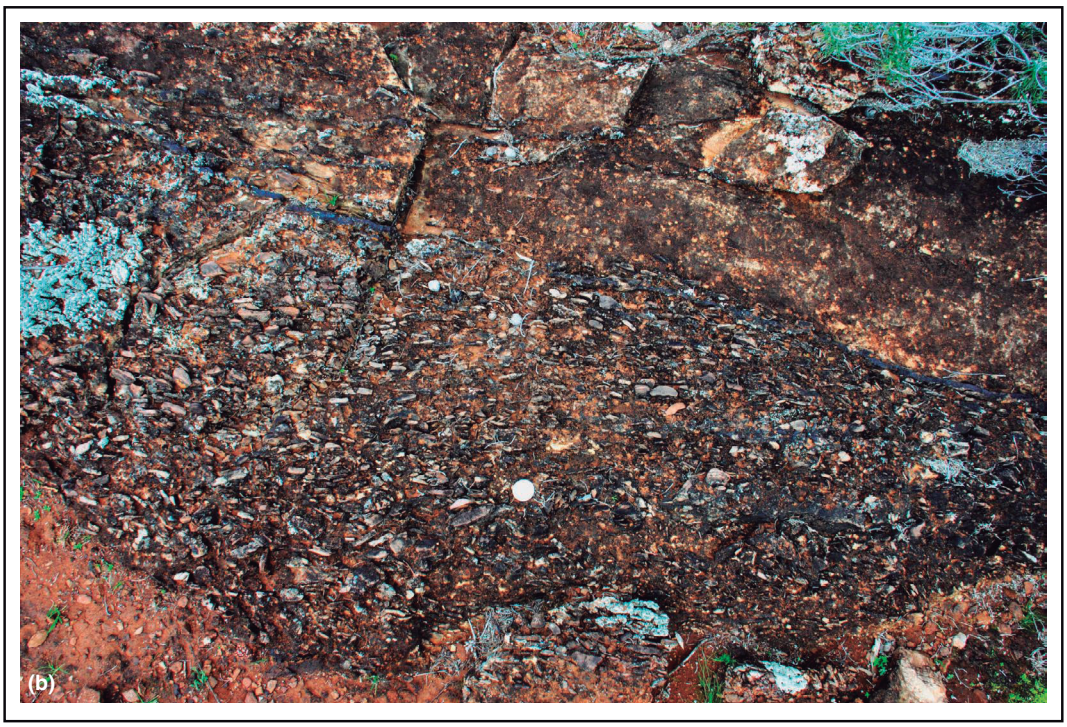

FIGURE 11 (a) Geological map of the SE flank of the South Angepena diapir (SA) and the overlying sequence in the Mount Hack minibasin (MH). Notice the presence of caprock along the eastern salt-sediment interface and several composite halokinetic sequences with strata rotating upwards and thinning towards the diapir within several hundred metres of the salt. Dotted lines in the Pound Subgroup denote mapped unconformable conglomeratic bodies described in the text. Colour legend and labels as in Figure 6. See Figure 6 for the location of this map in the subregional context. (b) Field picture of the elongated fabric facies (*chips*) interpreted as caprock (see coin for scale). See the white asterisk inside the black circle on the map above for location

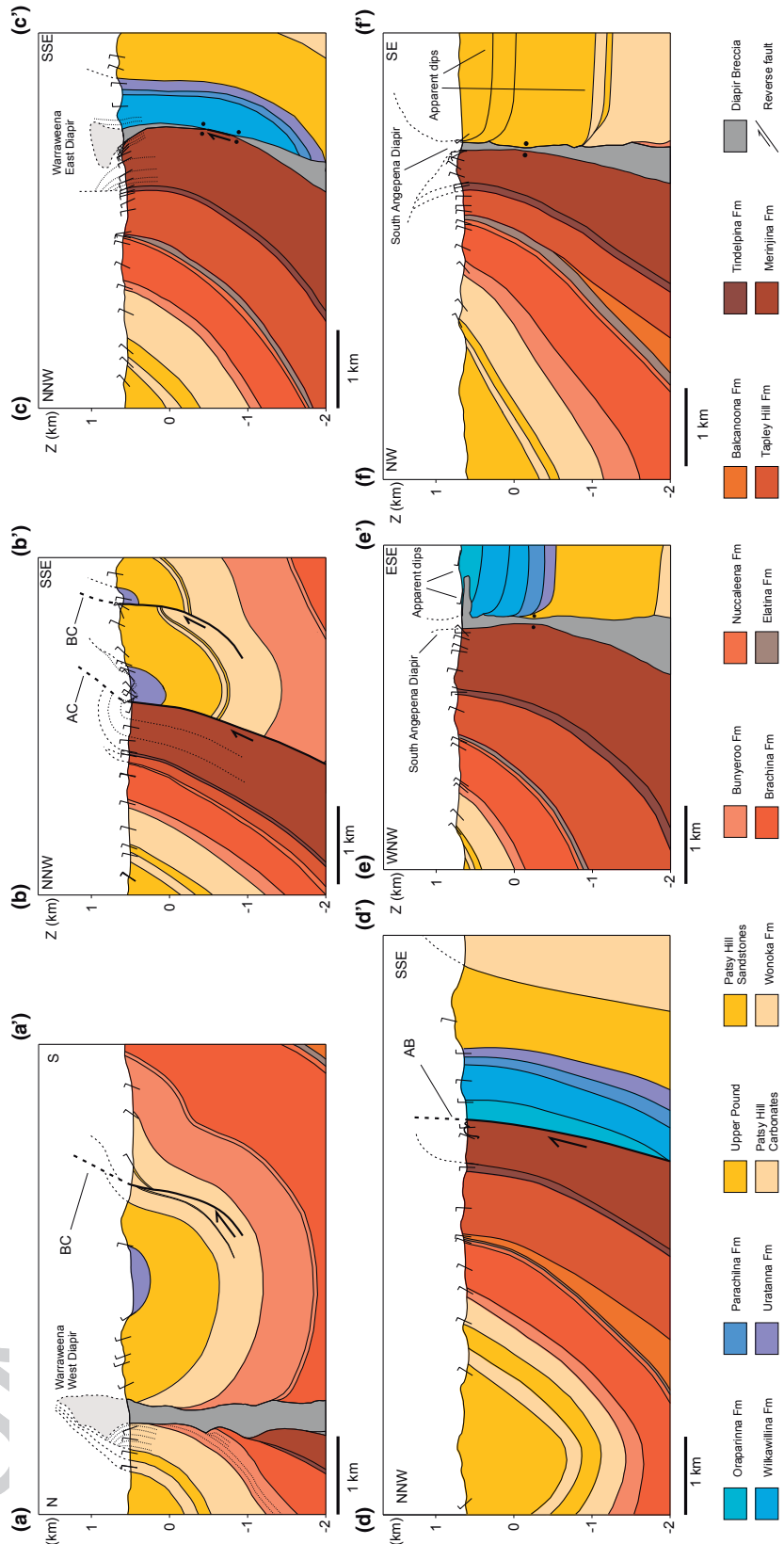

FIGURE 12 Vertical cross sections constructed from field data and observations (see Figure 6 for location). Dashed lines indicate inferred interpretation above ground based in part on projection from out of the plane, dotted lines indicate bedding traces. Colour legend and labels as in Figure 6

COLOUR online, B&W in print

west-dipping strata fold abruptly to overturned NNE dips about 50 m from the breccia, with the overturned limb disappearing rapidly near the last remnant of the Callanna breccia where it transitions to fault AC (Figure 7a). Fourth, the geometry near the south-western prong of Warraweena East is characterised by complex short-wavelength (ca. 50–60 m) folds with overturned beds adjacent to the Callanna breccia. The traces of these tight overturned folds are about 100- to 200-m long, are within 50–100 m from the breccia and intersect it at low angles. Finally, at the southwestern tip of Warraweena East, adjacent to the lateral transition from the Callanna breccia to fault BC, there is a rapid decrease in bedding dip from near vertical to moderate dips to the north.

4 | INTERPRETATION OF FIELD GEOMETRIES AND SURFACE DATA

4.1 | Callanna-brecciated bodies as passive diapirs

We interpret the Warraweena West, Warraweena East and South Angepena-brecciated bodies as passive salt diapirs growing from at least the Ediacaran Series (deposition of the Wilpena Group) well into the Early Cambrian (Hawker Group). The main evidence supporting this interpretation includes: (a) intra-Callanna deformation, such as both brecciated (chaotic) and well-layered, intensely folded blocks, similar to intra-salt deformation described in other basins (e.g. La Popa basin, Rowan et al., 2003; the Spanish Prebetics, Rubinat, 2012); (b) the presence of mm to cm halite crystal moulds (hoppers, according to arguments presented in Coats & Preiss, 1987); (c) interpreted lateral caprock (Giles et al., 2012; Jackson & Lewis, 2012) along the eastern boundary of the South Angepena iaper (Figure 11a), as elaborated below; (d) a general lack of small-scale (i.e. metre-scale or smaller) deformation in strata flanking the Callanna breccia bodies, suggesting that the Callanna lithologies were weaker than the surrounding rocks at the time of deformation (i.e. larger percentage of evaporites in the Callanna; see Rowan et al., 2020); (e) flanking folds, unconformities and conglomerates that we interpret as composite halokinetic sequences (CHS; see Giles & Rowan, 2012), displaying thickness and facies changes away from the Callanna interface and (f) short-distance (tens of metres) changes of geometry/structural style in the areas where the Callanna breccia thins out, suggesting rapid changes in structural style between areas across diapirs and areas where country rocks were not pierced by salt. Our interpretation is in line with similar structures seen elsewhere in the Flinders Ranges and interpreted as long-lived passive diapirs and salt sheets (Dalgarno & Johnson, 1968; Dyson, 1996; Hearon, Rowan, Giles, et al., 2015; Kernen et al., 2012, 2019; Rowan et al., 2019). The following paragraphs summarise the field-based evidence supporting our interpretation of the Callanna-brecciated bodies, along with specific traits that reveal more about their evolution as passive diapirs.

The clearest indication of passive diapirism at Warraweena West is the folding of the Wonoka Fm. on the north-eastern flank. Because the strata generally dip steeply to the NNW, the map view is effectively a cross-sectional view. This is confirmed by calculating the orientation of the salt-sediment interface using the method in Hearon, Rowan, Giles, et al. (2015): The resulting near-vertical present-day orientation yields a pre-Delamerian diapir flank dipping 40º to the NE. The lower Wonoka strata form a hook halokinetic sequence fossilised by the upper Wonoka and Pound, which thin over the top of the diapir (as inferred from Figures 6, 8 and 12a). In contrast, the Brachina and Bunyeroo fms. beneath the Wonoka are folded down onto the Umberatana-Wilpena unconformity (Figure 8). This fold might be the continuation to the NW of the anticline within the Merinjina Fm., northeast of fault AC, or it might have formed due to dissolution of a salt wing originally emplaced at the level of the unconformity. There is no evidence of passive diapirism in the Pound Subgroup at the southern side of Warraweena West (i.e. no apparent change in bedding morphology between areas adjacent to the Callanna and areas along fault AC, as seen on Figure 8), but since the diapir was buried by late Wonoka time, the salt-sediment interface here is probably a later thrust-related juxtaposition of the diapir against the Pound Subgroup.

At Warraweena East, we do not see clear evidence of passive diapirism in the bedding of either the Merinjina Fm. on the north side or the Cambrian strata on the south side (i.e. no apparent halokinetic folding nor significant changes in structural geometries across the Callanna; Figure 12c). However, the western flank (i.e. eastern end of Domain C) contains evidence of passive rise in the form of near-diapir halokinetic folds within the Pound Subgroup (Figure 7a). Diapir growth might have started earlier as seen on the northeast side of the Warraweena West diapir, but these levels are not exposed in Domain C. The original orientation of the salt-sediment interface cannot be calculated accurately because of its location at the steeply plunging termination of the Cadnia Syncline.

The best evidence of passive diapirism is along the south-eastern flank of the South Angepena diapir, where multiple CHS are interpreted in the Wilpena (Bunyeroo, Wonoka and Pound fms.) and Hawker units (Figures 6, 9, 11 and 12e,f). Observed features typical of CHS include: strata that turn up and thin within 300–400 m of the diapir edge; stacked local unconformities that intersect the edge of salt at cusps and poorly sorted conglomerates (interpreted as debris flows) that thin away from the diapir and contain clasts probably derived from both non-evaporite lithologies of the Callanna Group

(dark meta-sediments and meta-igneous rocks) and from the diapir roof (dark carbonate and dolomitic blocks). The geometries show that these are wedge halokinetic sequences that stack into tapered CHS (Giles & Rowan, 2012). The original orientation of the Callanna–Pound interface is calculated to have been near vertical.

Other aspects of the South Angepena diapir warrant mention. First, the band containing chips of silicified dolomite along the south-eastern interface (Figure 11b) is interpreted as carbonate caprock (see arguments presented in Giles et al., 2012; Kernen et al., 2019) that formed periodically at the top of the diapir due to halite dissolution in late Wilpena

COLOUR online, B&W in print

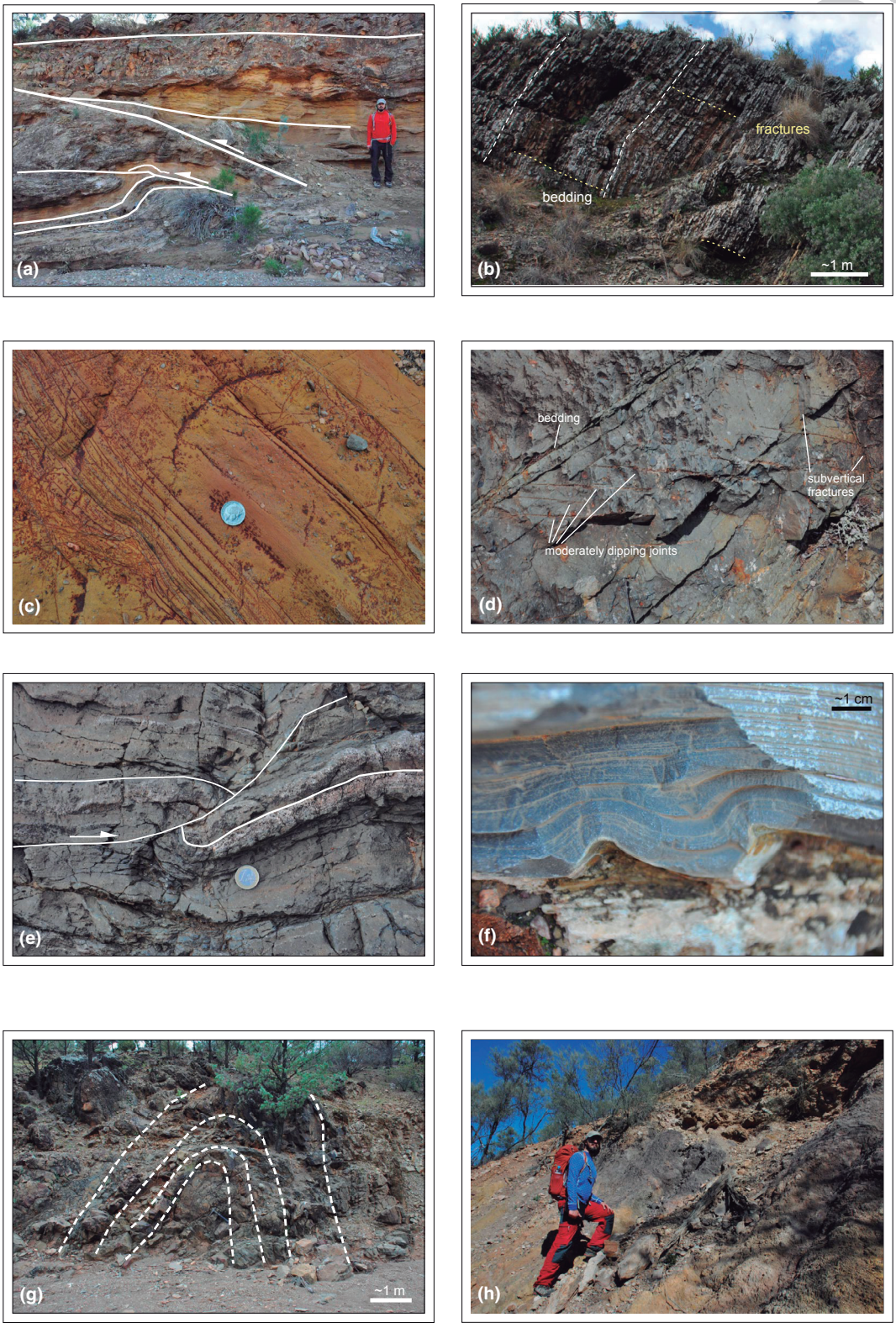

FIGURE 13 Examples of small-scale deformation across different domains. (a) Regional background deformation by thrust imbricates and detachment folding in the Pound Subgroup, near the Mount Goddard Syncline axis; (b) regional background deformation by bedding-perpendicular fractures in the Wonoka Fm. (interpreted lines are just a few examples of the centimetre-spaced strata-perpendicular fractures); (c) well-laminated layers of the Merinjina Fm. near the South Angepena diapir showing little internal deformation; (d) decimetric layers of the Merinjina Fm. displaying tensile joints oblique to bedding and filled with quartz crystals near the Warraweena East diapir (see coin in the centre for scale); (e) centimetre-scale folding and reverse faulting in the Merinjina Fm. near the weld at the southern termination of the South Angepena diapir, where the Callanna breccia is less than 50-m thick; (f) centimetre-scale concentric folding in the Oraparinna Fm., just east of the weld (Callanna breccia is ca. 75 m in map thickness); (g) metric-scale anticline in the Merinjina Fm., near fault segment AB (see hammer at the core of the anticline for scale); (h) highly altered and chaotic sediments in the fault zone of fault AB (stratigraphy, bedding and structural features are indistinguishable due to large internal shear along the fault). See Figure 6 for approximate location of a and b, Figure 10 for approximate location of c, Figure 8 for approximate location of d and Figure 9 for approximate location of e to h

time. Second, the small protrusion of Callanna breccia into Cambrian strata (Figure 9) is interpreted as a salt wing emplaced at the level of a CHS boundary (see Rowan, 2017, Figures 10a and 12e). Third, we interpret that the near-salt anticline affecting the Umberatana along the SW side of the South Angepena diapir (Figure 10) was not caused by halokinetic drape folding. Although unclear, we hypothesise that its origin may be due to either: (a) remnants of pre-existing folding before passive diapir rise juxtaposed it against salt; (b) fault-related folding away from the salt with strata on one side of the fault subsequently juxtaposed against the salt by ongoing fault slip (see Rowan et al., 2020); or (c) shortening-related deformation against non-evaporitic Callanna Group rocks.

4.2 | Linking structures and discrete diapirs versus squeezed salt wall

As shown in Figure 14, the linear to arcuate structures linking and extending away from the diapirs can be interpreted as either faults or secondary salt welds. In the first scenario, the current geometry of the Warraweena area would be the result of three discrete, pre-existing diapirs that were squeezed and linked by thrust faults during Delamerian shortening (Figure 14a). An alternative interpretation is that a 15-km-long salt wall was shortened and partly welded during the Delamerian Orogeny, resulting in three salt bodies connected by secondary welds (Figure 14b), a variation on Q-tip structures (Rowan & Vendeville, 2006). Both models necessarily imply the presence of complete or incomplete (i.e. less than 50 m of salt thickness) secondary welds, either just off the ends of the diapirs currently seen on maps (Figure 14a) or formerly, all along the linking structures (Figure 14b). Intermediate scenarios are also possible, in which either pair of diapirs represents an original wall and the third was an isolated diapir.

Several observations help to elucidate whether the linking structures are faults or secondary welds. First, no remnants of Callanna breccia (non-evaporite blocks) were identified along the linear structures linking the diapirs, despite their occurrence on documented welds in the Flinders and Willouran ranges (e.g. Dyson, 2005; Dyson & Rowan, 2004; Hearon, Rowan, Giles, et al., 2015; William et al., 2019). Second, halokinetic sequences are associated with the discrete diapiric bodies but are not found along the linking structures. Third, the areas between the diapirs have hectometre-scale anticlines in the upthrown (northern) block (Figures 7 and 12b,d), in contrast to areas adjacent to the brecciated bodies. Finally, an increase in small-scale deformation, mostly in the form of fractures and cleavage, is observed in areas in between the brecciated bodies along the linking structures, although this admittedly could have been generated after welding. Therefore, although we cannot completely rule out their origin as a formerly continuous salt wall (Figure 14b), the preponderance of evidence and the clear distinctions at not just one, but every scale of observation, lead us to interpret the linking structures as reverse faults (Figure 12b,d) that formed and connected the three discrete diapirs during the Delamerian Orogeny (Figure 14a). Similarly, we interpret fault BC (Figure 12b) as a thrust branching off the SW termination of the Warraweena East diapir. The faults are interpreted as steep (nearly vertical) south-directed reverse faults, where the hanging wall (northern block) is structurally higher than the footwall (southern block). Indications of southward reverse transport direction are also supported by the lack of Hawker Group sediments in the Mount Goddard Syncline (Domain A), structurally higher than Domains B and C, as well as the apparent overthrusting of the Mount Hack Syncline. We interpret the hectometre-scale anticlines in the upthrown block of Domain A near the fault segments as hanging-wall fault-related folds, widely described in fold and thrust belts all over the planet (e.g. Dahlstrom, 1970; Grasemann et al., 2005; Medwedeff & Suppe, 1997; Suppe, 1983, 1985).

The transition from diapir to reverse fault happens over short distances, often within less than 200 m along the fault trend (Figure 7a). A repeated pattern is that the map-view width of the diapir decreases to 100 to 15 m in the diapir terminations, narrows further to zero and transitions into a reverse fault where no Callanna breccia is observed. According to published definitions of welds (Hudec & Jackson, 2011;

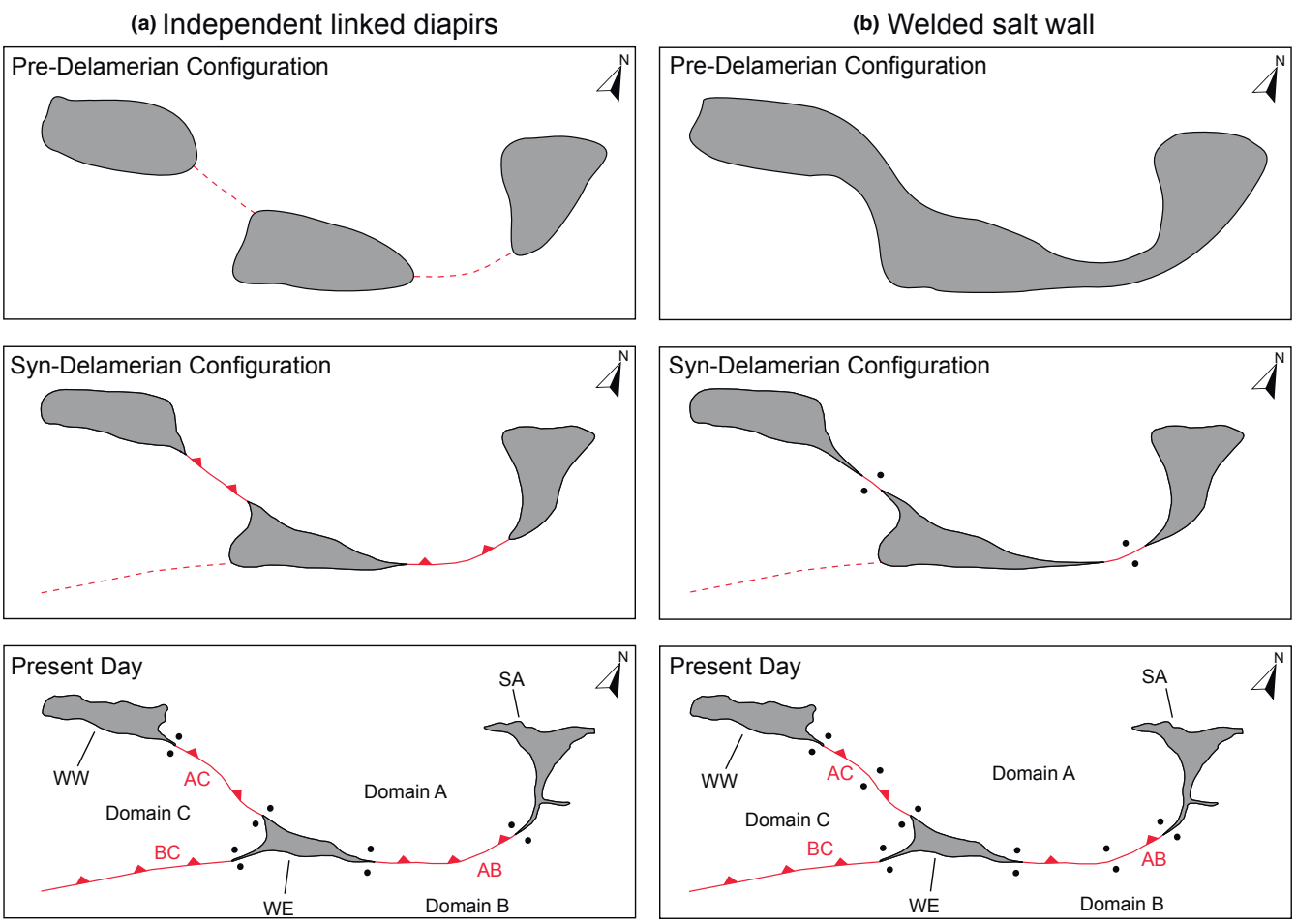

FIGURE 14 Conceptual evolutionary models in map view, assuming two possible end-member scenarios: (a) diapirs initiated as three independent structures, being later squeezed and developing lateral short welds that were linked by reverse faults and (b) diapirism initiated in the form of a salt wall that was later squeezed shut in places and eventually developed south-directed reverse fault segments along the welds. MG, Mount Goddard Syncline; MH, Mount Hack Syncline; SAD, South Angepena Diapir; WED, Warraweena East Diapir; CS, Cadnia Syncline; WWD, Warraweena West Diapir

Jackson & Hudec, 2017; Rowan & Ratliff, 2012; Wagner & Jackson, 2011), the salt bodies with widths of up to 50 m are classified as incomplete welds.

A good illustration of how this transition impacts both meso- and large-scale deformation in adjacent strata is provided by the Merinjina Fm. along the southern flank of Domain A. Along fault AC, strata form a hanging-wall anticline that is truncated by the fault (Figures 8 and 12b). Here, decimetre- to metre-scale tight folds within 200 m of the fault, increased fracture intensity and a minor shear fabric are interpreted as associated with fault development. Adjacent to the Warraweena East diapir, however, the Merinjina Fm. forms an overturned panel (Figure 12c) and there is no increase in small-scale deformation above background levels. A similar transition is seen from fault AB (Figure 12d) to the South Angepena diapir (Figures 9 and 12e,f). Here, because the Callanna breccia has a map width ranging from 0 to 100 m, it forms a combination of narrow diapirs and discontinuous weld. Increased small-scale deformation suggests that strain can be imparted to flanking strata before complete welding (e.g. intra-Callanna non-evaporitic lithologies might have transferred strain to flanking strata before complete welding occurred; see Davies et al., 2010).

To sum up, the structures in the Warraweena area are interpreted as a system of three squeezed diapirs that are locally welded at their tips and linked by steep, south-directed reverse faults and one branching imbricate. The diapirs rose passively since at least the Ediacaran and were shortened during the Delamerian Orogeny. Contraction resulted in the squeezing of the diapirs and folding and thrusting of the surrounding strata.

4.3 | Subsurface interpretation

Although no subsurface information is available, the observations and structural relationships observed at the surface give us hints about the geometry of the strata

and dividing structures at depth. One tool is that the steeply dipping bedding attitudes mean that the map often constitutes an approximate cross-sectional view when examined from a direction perpendicular to the strikes. Examples include viewing the northeastern flank of Warraweena West from the SE; viewing the entire southern limb of Domain A also from the SE and viewing the eastern flank of the South Angepena diapir from the NNE (Figure 6).

Another tool is to use the stratal dips to constrain the dips of the reverse faults. Because reverse faults almost always cut up-section relative to both hanging- and footwall strata, the faults are most likely steeper than the adjacent bedding. This, combined with the overall northward convex surface expression and the fact that Domain A is structurally higher than the others, suggests that the faults dip very steeply to the north (Figure 12b,d). The dips may decrease at depth, especially where the faults presumably merge with the autochthonous Callanna rocks at triangular pedestals (Figure 5). Moreover, the lower parts of the reverse faults may be welds if there were originally deep salt ridges connecting the diapirs.

The Warraweena East diapir was probably also vertical (Figure 12c) since it is flanked by two near-vertical faults (i.e. fault AC, Figure 12b; fault AB, Figure 12d). We depict the other diapirs in the same way (Figure 12a,e,f), although some tilting along with the strata of Domain A cannot be ruled out. Could the diapirs be squeezed shut and welded at depth as a consequence of Delamerian contraction? This would depend in part on the original geometry of the diapirs, which remains unknown; nevertheless, we depict local welds at depth (Figure 12).

In contrast to the other domains, the footwall (Domain B) of faults AB and BC and the Warraweena East diapir is not parallel to the bounding structures. The Mount Hack Syncline is truncated by the thrust system (Figures 6, 9 and 12), suggesting that the Mount Hack may have been a pre-existing fold, later cut by the dividing structures. Moreover, given that fault BC dies out in the stratal panel that forms the southern limb of both the Mount Hack and Cadnia synclines (see southwestern sector of Figure 6, where the fault segment BC dies out to the SW), the Mount Hack and Cadnia Synclines are likely to be the same structure at depth (Figure 12a), partly overridden by the south-directed relative movement of Domain A.

5 | DISCUSSION

As expounded in the previous section, we interpret the three Callanna-brecciated bodies in the Warraweena area as passive salt diapirs growing diachronously from at least the Ediacaran Series (deposition of the Wilpena Group) well into the Early Cambrian (Hawker Group). However, how did these diapirs evolve in three dimensions through time? What are the plausible alternative scenarios that can be considered leading to the geometry and distribution of meso- and small-scale deformation that we observe in the field? What are the key lessons learned in Warraweena that can be applied in other global salt provinces where field exposures are not available? In this section, we discuss different alternatives for the formation and evolution of the shortened passive diapirs connected by linking faults, as well as pointing to the applicable learnings and implications for seismic interpretation and prospectivity that can be used in similar settings elsewhere.

5.1 | Three-dimensional geometry and evolution

The results of our work illustrate the geometry and evolution of squeezed diapirs, associated reverse faults and flanking minibasins in the Northern Flinders Ranges of South Australia. The salt-sediment relationships and the composite halokinetic sequences adjacent to all three diapirs indicate that passive diapirism was ongoing during the Ediacaran and lasted until at least the Early Cambrian. Thus, passive diapirism and shortening may have coexisted if the onset of the Delamerian Orogeny occurred during the latest Neoproterozoic (Jenkins, 1990; Lemon, 1988; Rowan et al., 2019; Rowan & Vendeville, 2006; Turner et al., 2009). But when did passive diapirism initiate? We see no evidence of passive diapirism in the Umberatana Group adjacent to any of the diapirs, and the prominent base-Wilpena unconformity in Domain A separates different geometries in the Umberatana and Wilpena strata, with the former thinning and folding gently up towards the Warraweena West and South Angepena diapirs (Figures 5 and 6). Thus, we speculate that Umberatana strata thinned onto precursor salt pillows and that base-Wilpena erosion of the highs thinned the roofs enough to allow the salt to breakthrough in a brief phase of active diapirism (see Rowan & Giles, 2020) and subsequently start growing passively during Wilpena time, with the consequent development of composite halokinetic sequences. In this scenario, the three synclines defining Domains A, B and C started as salt-withdrawal minibasins, with the underlying salt first moving into pillows and subsequently into the growing diapirs.

Again, we interpret three distinct passive diapirs rather than one salt wall (or one shorter wall and one separate diapir). Admittedly, some of the observed differences between features flanking the breccia bodies and those adjacent to the linking structures are not diagnostic. For example the increase in small-scale deformation along

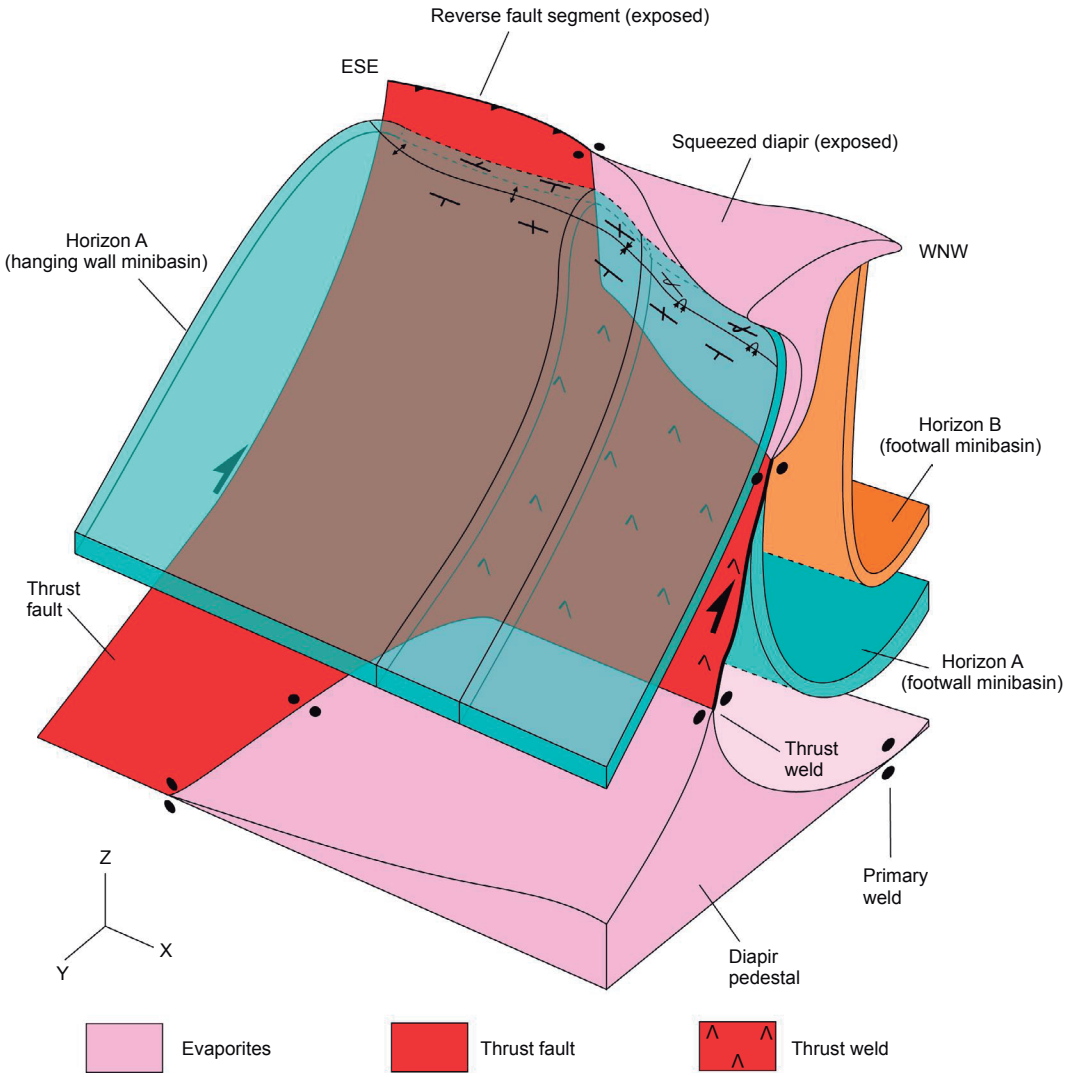

FIGURE 15 3D model showing the lateral transition from squeezed diapir to weld to thrust fault and the changing structural style in the hanging wall minibasin. Salt is depicted in pink. Horizons A and B depicted in the figure are merely illustrative and are not related to any specific stratigraphic marker. Footwall configuration is based on the geometry seen in Warraweena West, although different footwall configurations are seen in other sectors of the studied area

the linking structures could have been generated by post-welding weld-parallel slip. And the lack of halokinetic sequences in some areas can be explained by the strata being pre-diapiric (as interpreted for the Umberatana strata along the southern flank of Domain A) or as having been juxtaposed against the Callanna only during late thrusting (as possible for the footwall Cambrian strata of Fault AB). Instead, two considerations lead us to reject the salt-wall option. First, the complete lack of Callanna breccia along any part of the linking structures strongly suggests that salt was never present in these locations. Although one could argue that there were parts of the wall with only halite and no stringers, this would be highly coincidental along the almost 3-km-long faults AB and AC. Second, the change in geometry in the Merinjina Fm. adjacent to the breccia bodies (steepening strata) versus the linking structures (anticlinal folds) is striking (Figures 12 and 15) and is compatible with squeezing of a diapir versus fault-related contractional deformation.

The Delamerian Orogeny resulted in shortening being accommodated in three different ways. First, the minibasins evolved into tight synclines, with the limbs rotating to near-vertical. Second, the formation of south-directed, steep reverse faults led to the Mount Goddard minibasin (Domain A) being thrusted over the combined Mount Hack-Cadnia minibasin (Domains B and C). Third, the shortening squeezed the three diapirs enough to form short (ca. 200 m) secondary welds at their lateral terminations where they transitioned into the steep reverse faults. The corresponding transition from steepened bedding to hanging-wall anticlines (Figure 15) was gradual as no faults were observed separating the two styles.

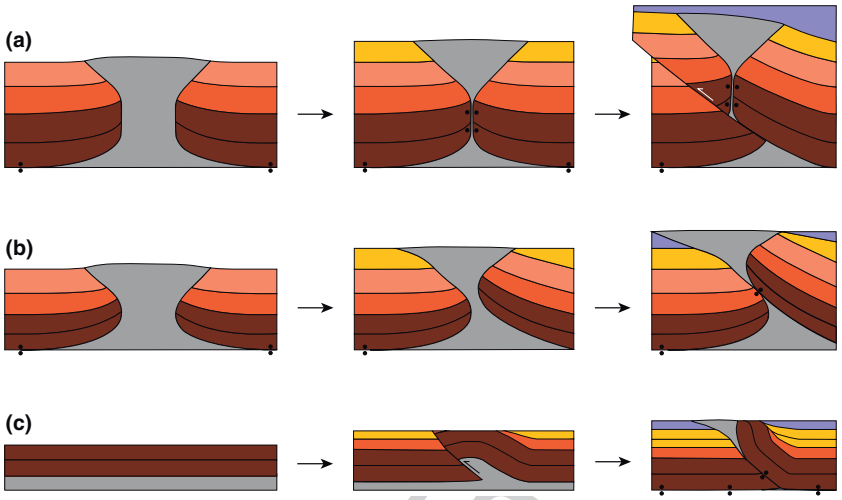

FIGURE 16 Schematic diagrams showing end-member structural styles of thrusted diapirs: (a) decapitated diapir; (b) thrust-welded diapir and (c) welded source-fed thrust. Modified after Rowan (2020)

5.2 | Shortening of pre-existing diapirs: Field examples versus published models

Shortening of salt stocks and walls displaces salt and may result in pinching-off of their necks with complete exhaustion of salt supply and the development of secondary welds (Callot et al., 2007, 2012; Hudec & Jackson, 2007; Pichel et al., 2017; Rowan & Vendeville, 2006; Vendeville & Nilsen, 1995). Their subsequent evolution depends in part on the geometry of the salt structure at the time of welding. Three different modes of secondary weld formation and evolution are presented and discussed here (Figure 16; Rowan, 2020). For vertical secondary welds with relatively small pedestals (Figure 16a), additional shortening is accommodated by the development of a thrust fault that decapitates the diapir and separates it from its pedestal, carrying the weld and the shallower section of the diapir in the hanging wall (Callot et al., 2007; Dooley et al., 2009; Duffy et al., 2018; Ferrer, 2012; Granado et al., 2018; Pichel et al., 2017; Roma et al., 2018). In contrast, a flaring diapir and large pedestal may lead to an inclined thrust weld, with the hanging-wall minibasin thrust over the footwall minibasin (Figure 16b; Jackson et al., 2008; Rowan, 2020). Originally leaning diapirs may also form inclined thrust welds. Pre-existing diapirs are not required for thrust welds; they may also develop by squeezing salt in the hanging wall of a source-fed thrust (Figure 16c; Rowan, 2020). The thrust may emanate from either an undeformed salt layer (as shown in Figure 16c) or a precursor salt pillow or ridge.

In the light of the evolutionary models presented above (Figure 16) and the geometries interpreted in the field, we discuss three different possibilities to generate the discrete diapirs connected by reverse fault segments seen in Warraweena. First, decapitation of previously welded vertical diapirs by a thrust fault (Figure 16a) would result in diapirs being passively transported in the hanging wall, with the diapirs at a distance from where the thrust fault is exposed (Figure 17a). Alternative geometries have been generated in models (Duffy et al., 2018),

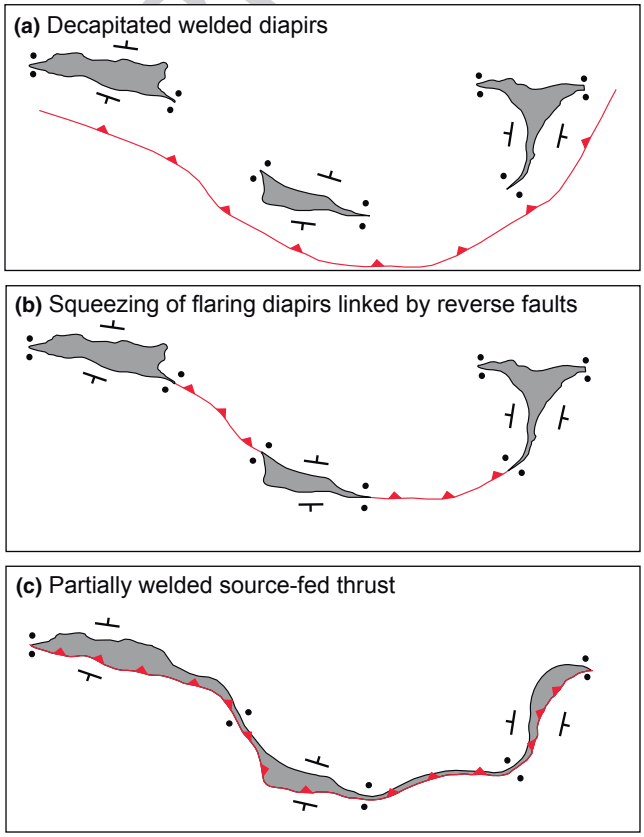

FIGURE 17 Schematic sketch illustrating hypothetical field exposure of the three thrust weld modes shown in Figure 16: (a) decapitated diapirs; (b) flaring diapirs linked by short thrust welds and reverse fault segments and (c) partially welded source fed thrust

with the faults curving sharply, either towards the foreland or towards the hinterland, to intersect the diapirs. In any case, we see none of these patterns and thus reject an interpretation of decapitated diapirs. Second, flaring diapirs squeezed during the Delamerian Orogeny and connected by reverse faults (Figures 16b and 17b) would generate the observed contractional styles and be compatible with the halokinetic folding seen on

each independent diapir. Third, emplacement and partial welding of a source-fed thrust followed by hanging-wall erosion and salt breakout (Figure 16c) would result in similar geometries to what we observe (i.e. linear to arcuate structure with variable width). However, in such a case the connecting structures observed at the surface would be welds (Figure 17c) instead of steep reverse faults where no remnant salt exists (Figure 17b). In addition, an origin as a source-fed thrust (Figures 16c and 17c) is incompatible with the evidence for passive growth of the three diapirs, and thus this option can also be eliminated. Therefore, we conclude that the second scenario where the squeezing of three discrete passive diapirs and the formation of linking reverse faults is the best-fitting evolutionary model that would explain our field observations (Figure 17b). Squeezing of pre-existing model salt walls produces map patterns that are remarkably similar to those of the Warraweena area (e.g. figures 9.25c, d in Jackson & Hudec, 2017).

There are, however, a number of differences between model geometries, whether analogue, numerical or conceptual, and what we see in the field. The most obvious is the moderately dipping bedding of flanking minibasins in the models (e.g. Figure 16 of this manuscript, figure 6 in Pichel et al., 2017 or figure 8a in Roma et al., 2018) versus the steeply dipping (at least at the surface) bedding observed in Warraweena (Figure 12). In sandbox modelling this is a natural limitation of using cohesionless sand as an analogue of the sedimentary cover. In numerical models, though, it is usually related to the boundary conditions or the limitations of the code at hand (i.e. DEM vs. FEM vs. geometric relationships between horizons and faults).

Similarly uncommon in modelling is the steep dip documented in the surface expression of the reverse faults in Warraweena. Although steep reverse faults have been observed on seismic (Figure 1), they are rare in analogue models (see diapir 3 in figure 5a of Rowan & Vendeville, 2006 or figure 11.15a in Jackson & Hudec, 2017). Experimental results do not reproduce the nearly vertical faults along with vertical to overturned bedding such as that documented in Warraweena. Moreover, near-vertical reverse faults and hanging-wall strata are rare in most orogenic belts unless there has been steepening by later footwall imbricates. There are exceptions in the case of isolated minibasins, mostly surrounded by salt, that rotate to very steep attitudes (e.g. Duffy et al., 2020; Kergaravat et al., 2017), but that explanation is inapplicable due to the large anticlines bounding the synclines to the north and south of the study area (Figure 5).

We suggest that several factors may have influenced the development of the steep bedding and faults. First, although not reproduced in models, we cannot rule out that the existence of pre-existing vertical salt walls might have favoured the generation of steep faults once the diapirs were squeezed enough. These faults might decrease in dip away from the diapirs unless they are connecting closely spaced diapirs, as is the case in the Warraweena area where the linking faults are only ca. 2.5-km long. Second, there may have been a component of strike-slip movement along the faults, due to either the regional stress field or local vertical-axis rotation of minibasins, but we have no supporting evidence for either of these. Third, the steep attitudes may have been due to increased tightening of the synclines as a consequence of continued shortening after diapirs were mostly squeezed shut. Alternatively, the continuation of shortening may have led to the folding of the reverse faults, but this would also necessitate that the footwalls were deformed unless the footwalls had adequate salt to absorb any such strain.

5.3 | Small-scale deformation in Warraweena

Because the study area is in an orogenic belt, there are background small-scale contractional structures seen in areas away from diapirs and faults. The deformation is characterised by decimetric to metric thrusts and folds accommodating layer-parallel shortening; a weak tectonic foliation mostly subparallel to steep bedding; unmineralised joints and veins. The latter includes minor bedding-parallel veins compatible with flexural-slip folding and bedding-perpendicular fractures, most of which accommodate the along-strike extension that is common in fold-and-thrust belts (Figures 13a,b and 18). Deformation styles and intensity vary non-systematically with, for example fractures occurring in swarms.

There is no significant increase in fracture intensity near diapirs (Figures 13c,d and 18), although there is a tendency for joints to be less organised. However, this occurs primarily in the massive tillite and thus might reflect mechanical control by the stratigraphy. Adjacent to incomplete welds, additional deformation is observed in the form of more common folding and fracturing (Figures 13e,f and 18). This probably reflects the tendency of strain to be recorded in wall rocks when the salt gets thin (Davies et al., 2010). Finally, areas across faults are characterised by a marked increase in fractures, folds and cleavage, often masking bedding/lamination due to large internal strain (Figures 13g,h and 18). In general, the lack of increased small-scale deformation near salt structures but an increase near faults is entirely consistent with field observations in other salt provinces such as La Popa Basin in Mexico (Rowan et al., 2003), the Spanish Pyrenees and the Zagros Mountains in Iran (see Rowan et al., 2020 for a review).

5.4 | Implications for seismic interpretation and prospectivity in other salt basins

Seismic interpreters and exploration geoscientists working on compressional salt provinces commonly face difficulties to interpret the geometry and nature of three-way truncations against

COLOUR online, B&W in print

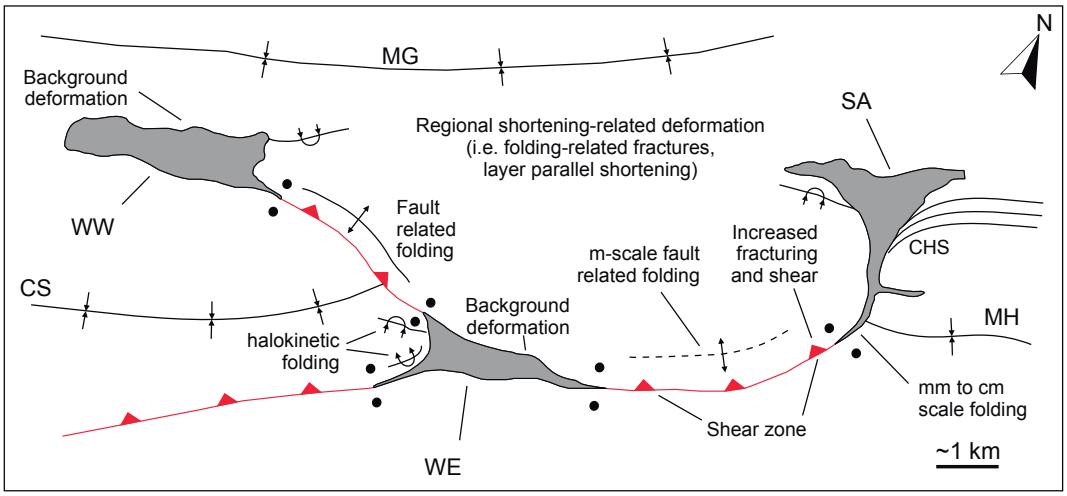

FIGURE 18 Summary sketch of structural domains, dividing structures (diapirs, welds and thrusts), features and small-scale deformation styles seen in the different sectors of Warraweena, Northern Flinders Ranges of South Australia. Labels as in Figure 6

squeezed salt, welds or faults. Their commonly steep morphology and sub-seismic resolution thickness (e.g. Figure 1), as well as other limitations associated with seismic acquisition and processing (e.g. overmigration, use of inaccurate velocity models or inappropriate dip illumination), make the characterisation of these structures a challenge. A correct understanding of their geometry and evolution has important implications for the characterisation of such play types in petroleum systems of subsurface salt basins (e.g. the Gulf of Mexico, offshore Morocco or offshore Angola, among others). Is it one continuous salt wall, now partly welded, or are they different discrete diapirs linked by reverse faults? If the latter, what does the transition from diapir to weld and finally to fault look like in detail? Is there a variation in the pattern of small-scale (i.e. metric and below) deformation along strike? The geometric relationship between flanking strata and linking structures helps us to answer these questions, and is of paramount importance to predict not only trap geometry and volumetrics, but also enhancement of hydrocarbon migration pathways and sealing mechanisms.

Field geometries exposed in the Warraweena area of the Northern Flinders Ranges help us in assessing what these structures look like, how they link laterally and transition into each other and what small-scale deformation patterns characterise each domain. A summary of traits and specific features at different scales as well as their lateral transition is provided in Figure 18. Passive diapir rise is typically characterised by the presence of composite halokinetic sequences (CHS) and diapir roof detritus deposited in flanking strata, instances of lateral caprock, as well as steepening of bedding in flanking minibasins towards the diapir as the salt edge is approached. Linking reverse fault segments commonly display hanging-wall anticlines of tens to hundreds of metres in wavelength with stratal dips decreasing towards the fault, as seen along the fault segment AC, or simply panels of fairly constant dip and minor folding as seen in fault segment AB (Figure 18). When trying to identify whether we are interpreting a flanking minibasin against squeezed/welded salt or simply a fault-related folded panel, these are the key geometric relationships between horizons, faults and salt to look for in seismic.

Before transitioning into reverse faults, diapirs thin to thrust welds. In the case of Warraweena East, these are short thrust welds, ca. 200-m long (Figure 8a). However, given that seismic resolution most likely will not image steep salt even 100- to 200-m thick, apparent thrust welds can be longer, as seen along the ca. 2-km-long continuation of the South Angepena diapir towards the south (Figures 9 and 11). Here, CHS are observed even in areas where the thickness of the mobile unit is nearly depleted (<75 m).

Finally, field observations in Warraweena teach us that the expected sub-seismic, small-scale deformation can be derived from the geometric relationships between flanking horizons and salt versus faults. If there is evidence of salt along the boundary (either imaged salt, CHS or just steepening dips), then only background (i.e. regional) levels of small-scale deformation would be expected (Figures 13c,d and 18) along with tentative presence of soft sediment deformation (e.g. syn-sedimentary slumping, convolute bedding, etc.). Where evidence for reverse faults is encountered (i.e. either hectometric-scale hanging-wall anticline formation, dips shallowing towards the boundary or simply panels of fairly constant dip), then increased small-scale folding, fracturing at high angle to the bedding and shear/damage zones along the fault would be expected (Figures 13g,h and 18). In areas of thin salt (<50 m) or welds, an intermediate scenario is likely to be encountered (i.e. both small-scale shear and folding; Figures 13e,f and 18).

Despite the analogies discussed above, there are also important differences to bear in mind between the salt features observed

in the Northern Flinders of South Australia and other salt provinces around the globe. First, as described in the Stratigraphy section, the origin of the Callanna Group breccia is interpreted to be a layered evaporite sequence comprising evaporites interbedded with siliciclastics, carbonate and igneous rocks, from which the evaporites are currently absent. Some other evaporitic units, such as the Louann Formation in the Gulf of Mexico or the Aptian layered evaporite sequence in offshore Brazil, for example are characterised by well-documented large percentages of evaporitic content, namely halite with varying amounts of other evaporites such as anhydrite, sylvite, carnallite or tachyhydrite, and at most insignificant quantities of strong non-evaporite layers (Fiduk & Rowan, 2012; Gamboa et al., 2008; Hazzard et al., 1947; Hearon, Rowan, Giles, et al., 2015; Jackson et al., 2014, 2015; Karner, 2000; Meisling et al., 2001; Rodriguez et al., 2018; Salvador, 1987). Despite this apparent rheological difference that might influence the mechanical response to sedimentary loading and shortening, the Callanna Group mobile unit seems to have behaved similarly to the evaporitic units in the aforementioned prospective basins. The lack of near-diapir deformation of flanking strata even in the presence of strong non-evaporitic stringers in the Callanna Group of the Northern Flinders makes us expect the described small-scale deformation patterns to be even more applicable in evaporite-rich salt basins such as the Gulf of Mexico or the South Atlantic margins.

6 | CONCLUDING REMARKS

The field exposures described in the Warraweena area of the Northern Flinders Ranges, South Australia, provide the rare opportunity to investigate one of the oldest examples of shortened salt bodies on Earth, within a salt basin that evolved for at least 300 million years. Salt structures in the study area grew as passive diapirs during the Neoproterozoic and Early Cambrian and were shortened during the Delamerian Orogeny, resulting in salt remobilisation, formation of short thrust welds and steep reverse faults linking diapirs. Increased shortening after the development of the thrust welds and reverse faults resulted in folding and southward overlap of one adjacent minibasin above the other. We also suggest that continued shortening after the formation of thrust welds and reverse faults may have led to the steepening and folding of strata in juxtaposed minibasins across the weld, and even the weld itself.

Using geological mapping, cross-section construction and structural models, we have analysed the geometry and evolution of three discrete diapirs in the area linked by subvertical reverse faults. The diapirs and linking faults separate the Mount Goddard minibasin to the north (upthrown minibasin) from the Mount Hack and Cadnia minibasins to the south (downthrown minibasins). The changing structural style of strata in the flanking minibasins has also been assessed, and forms a complex three-dimensional pattern where the geometry, dip and polarity of the bedding change between areas flanking diapirs and those adjacent to fault segments. The main takeaway messages are as follows:

- In areas near salt bodies, flanking strata are characterised by the presence of composite halokinetic sequences, instances of lateral caprock and an overall steepening of the bedding towards the salt edge.
- In areas near fault segments, minibasin strata exhibit either fault-related anticlines of tens to hundreds of metres in size, with dips decreasing towards the fault, or panels of roughly constant dip.
- The lateral transition from diapir to weld to thrust happens in a short distance, within barely 200 m, giving rise to short thrust welds at the diapirs' tips. Therefore, the structural style and geometrical relationships between minibasin strata, salt bodies and reverse faults change abruptly.
- Small-scale deformation in flanking minibasins also changes accordingly. Near diapirs, only background levels are observed, along with some instances of soft-sediment deformation. Welds have minor development of mm- to cm-scale folding, reverse faulting and fractures at high angle to the bedding. Near fault segments, we see a marked increase in metre-scale folding, fractures and cleavage, often masking bedding/lamination due to large internal strain.

The results of our research are useful in guiding and informing seismic interpretation of shortened diapirs and minibasins in global salt basins. Many of the field geometries described here are below seismic resolution and may help improve our characterisation of three-way closures and sub-thrust plays below allochthonous salt, particularly in the definition of trap configuration, assessment of hydrocarbon migration pathways and the sealing potential of secondary welds and associated thrusts.

ACKNOWLEDGEMENTS

This study has been funded by present and past corporate sponsors of the Salt-Sediment Interaction Research Consortium at The University of Texas at El Paso (BHP, BP, Chevron, ConocoPhillips, ExxonMobil, Hess, Kosmos, PGS, Repsol, Shell, and Total). ConocoPhillips is acknowledged for providing high-resolution satellite imagery of the field area. We appreciate the help of Kathryn Amos and the rest of the team at the Australian School of Petroleum at the University of Adelaide, who provided field equipment and guidance essential for the successful completion of the field work. We also thank Stony Steiner, caretaker of the Warraweena station, for his constant help and support during the 7 weeks we stayed in Warraweena conducting geological mapping and collecting data. Digital mapping was conducted in the field using FieldMove and FieldMove Clino applications. Midland Valley Exploration Ltd. (currently under Petroleum Experts Ltd.) is

acknowledged for provision of Move and FieldMove academic licenses to the University of Barcelona back in 2016–2017. We thank WesternGeco for permission to use examples shown in Figure 1. Constructive reviews from C.A.L. Jackson, J.I. Soto and an anonymous reviewer greatly helped to improve the manuscript, for which the authors are grateful.

PEER REVIEW

The peer review history for this article is available at https://publons.com/publon/10.1111/bre.12579.

DATA AVAILABILITY STATEMENT

The data that support the findings of this study are available from the corresponding author upon reasonable request.

ORCID

Oskar Vidal-Royo https://orcid.org/0000-0002-7957-5485

REFERENCES

Backé, G., Baines, G., Giles, D., Preiss, W., & Alesci, A. (2010). Basin geometry and salt diapirs in the Flinders Ranges, South Australia: Insights gained from geologically-constrained modelling of potential field data. *Marine and Petroleum Geology*, *27*, 650–665. https://doi.org/10.1016/j.marpetgeo.2009.09.001

Brun, J. P., & Fort, X. (2004). Compressional salt tectonics (Angolan margin). *Tectonophysics*, *382*(3–4), 129–150. https://doi.org/10.1016/j.tecto.2003.11.014

Burns, K. L., Stephansson, O., & White, A. J. R. (1977). The Flinders Ranges breccia of South Australia–Diapirs or décollement? *Journal of the Geological Society*, *134*(3), 363–384. https://doi.org/10.1144/gsjgs.134.3.0363

Callot, J. P., Jahani, S., & Letouzey, J. (2007). The role of pre-existing diapirs in fold and thrust belt development. In O. Lacombe, F. Roure, J. Lavé, & J. Vergés (Eds.), *Thrust belts and foreland basins. Frontiers in earth sciences*. Springer. https://doi.org/10.1007/978-3-540-69426-7_16

Callot, J.-P., Ribes, C., Kergaravat, C., Bonnel, C., Temiz, H., Poisson, A., Vrielynck, B., Salel, J.-F., & Ringenbach, J.-C. (2014). Salt tectonics in the Sivas basin (Turkey): Crossing salt walls and minibasins. *Bulletin De La Societe Geologique De France*, *185*(1), 33–42. https://doi.org/10.2113/gssgfbull.185.1.33

Callot, J.-P., Trocmé, V., Letouzey, J., Albouy, E., Jahani, S., & Sherkati, S. (2012). Pre-existing salt structures and the folding of the Zagros Mountains. *Geological Society, London, Special Publications*, *363*(1), 545–561. https://doi.org/10.1144/SP363.27

Coats, R. P. (1964). Large scale precambrian slump structures, flinders ranges. *Quaternary Geology Notes, Geological Survey of South Australia*, *11*, 1–2.

Coats, R. P. (1973). *COPLEY map sheet, South Australia geological survey geological atlas 1:250000 series, sheet SH 54–9*. Geological Survey of South Australia.

Coats, R. P. (2009). *ANGEPENA map sheet, geological atlas 1:100000 series, sheet 6636*. Geological Survey of South Australia.

Coats, R. P., & Preiss, W. V. (1987). The warrina supergroup. In W. V. Preiss (Ed.), *Geological society of Australia bulletin: The adelaide geosyncline – later proterozoic stratigraphy, sedimentation, paleontology, and tectonics* (Vol. 53, 43–72). Department of Mines and Energy, Geological Survey of South Australia.

Dahlstrom, C. D. A. (1970). Structural geology in the eastern margin of the Canadian Rocky Mountains. *Bulletin of Canadian Petroleum Geology*, *18*, 332–406.

Dalgarno, C. R. (1998). Extensional sedimentary regimes in the neoproterozoic of the adelaide geosyncline. Abstract No. 50. The Assembly and Breakup of Rodinia, Perth, September 1998.

Dalgarno, C. R., & Johnson, J. E. (1968). Diapiric structures and Late precambrian-early cambrian sedimentation in flinders ranges, South Australia. In J. Braunstein, & G. D. O'Brien (Eds.), *AAPG memoir 8. Diapirs and diapirism* (pp. 301–314). American Association of Petroleum Geologists.

Davies, R. K., Bradbury, W., Fletcher, R., Gavin, L., Welch, M., & Knipe, R. (2010). Outcrop observations and analytical models of deformation styles and controls at salt-sediment margins. AAPG Search and Discovery Article #90104, American Association of Petroleum Geologists.

Dooley, T. P., Jackson, M. P. A., & Hudec, M. R. (2009). Inflation and deflation of deeply buried salt stocks during lateral shortening. *Journal of Structural Geology*, *31*(6), 582–600. https://doi.org/10.1016/j.jsg.2009.03.013

Duffy, O. B., Dooley, T. P., Hudec, M. R., Jackson, M. P. A., Fernandez, N., Jackson, C. A. L., & Soto, J. I. (2018). Structural evolution of salt-influenced fold-and-thrust belts: A synthesis and new insights from basins containing isolated salt diapirs. *Journal of Structural Geology*, *114*, 206–221. https://doi.org/10.1016/j.jsg.2018.06.024

Duffy, O. B., Fernandez, N., Peel, F. J., Hudec, M. R., Dooley, T. P., & Jackson, C. A. L. (2020). Obstructed minibasins on a salt-detached slope: An example from above the Sigsbee canopy, northern Gulf of Mexico. *Basin Research*, *32*, 505–524. https://doi.org/10.1111/bre.12380

Dyson, I. A. (1996). A new model for diapirism in the Adelaide Geosyncline. *MESA Journal*, *3*, 41–48.

Dyson, I. A. (1998). The 'Christmas tree diapir' and salt glacier at Pinda Springs, central Flinders Ranges. *MESA Journal*, *10*, 40–43.

Dyson, I. A. (2005). Evolution of allochthonous salt systems during development of a divergent margin: The Adelaide Geosyncline of South Australia. In P. J. Post, N. C. Rosen, D. L. Olson, S. L. Palmes, K. T. Lyons, & G. B. Newton (Eds.), *Petroleum systems of divergent continental margin basins: 25th Annual GCSSEPM Foundation Bob F. Perkins Research Conference* (pp. 541–573). 11

Dyson, I. A., & Rowan, M. G. (2004). Geology of a welded diapir and flanking mini-basins in the Flinders Ranges of South Australia. In P. J. Post, D. L. Olson, K. T. Lyons, S. L. Palmes, P. F. Harrison, & N. C. Rosen (Eds.), *Salt sediment interactions and hydrocarbon prospectivity concepts, applications and case studies for the 21st Century: 24th Annual GCSSEPM Foundation Bob F. Perkins Research Conference* (pp. 69–89). 12

Escosa, F. O., Roca, E., & Ferrer, O. (2018). Testing thin-skinned inversion of a prerift salt-bearing passive margin (Eastern Prebetic Zone, SE Iberia). *Journal of Structural Geology*, *109*(February), 55–73. https://doi.org/10.1016/j.jsg.2018.01.004

Ferrer, O. (2012). *Salt tectonics in the Parentis Basin (eastern Bay of Biscay). Origin and kinematics of salt structures in a hyperextended margin affected by subsequent contractional deformation* (PhD dissertation). University of Barcelona, Barcelona. http://diposit.ub.edu/dspace/handle/2445/34935

Ferrer, O., Jackson, M. P. A., Roca, E., & Rubinat, M. (2012). Evolution of salt structures during extension and inversion of the Offshore Parentis Basin (Eastern Bay of Biscay). *Geological Society, London, Special Publications*, *363*(1), 361–380. https://doi.org/10.1144/sp363.16

Fiduk, J. C., Brush, E. R., Anderson, L. E., Gibbs, P. B., & Rowan, M. G. (2004). Salt deformation, magmatism, and hydrocarbon prospectivity in the Espirito Santo Basin, Offshore Brazil. In P. J. Post, D. L. Olson, K. T. Lyons, S. L. Palmes, P. F. Harrison, & N. C. Rosen (Eds.), *Salt sediment interactions and hydrocarbon prospectivity concepts, applications and case studies for the 21st century*. SEPM Society for Sedimentary Geology. https://doi.org/10.5724/gcs.04.24.0640

Fiduk, J. C., & Rowan, M. G. (2012). Analysis of folding and deformation within layered evaporites in Blocks BM-S-8 & -9, Santos Basin, Brazil. *Geological Society, London, Special Publications*, *363*(1), 471–487. https://doi.org/10.1144/sp363.22

Foden, J., Elburg, M. A., Dougherty-Page, J., & Burtt, A. (2006). The timing and duration of the Delamerian Orogeny: Correlation with the Ross Orogen and implications for Gondwana assembly. *The Journal of Geology*, *114*(2), 189–210. https://doi.org/10.1086/499570

Forbes, B. G. (1990). Geology of the willouran ranges. In J. B. Jago, & P. S. Moore (Eds.), *The evolution of a late precambrian-early paleozoic rift complex: The adelaide geosyncline* (Vol. *16*, pp. 68–84). Geological Society of Australia Special Publication, Geological Society of Australia Incorporated.

Gamboa, L. A. P., Machado, M. A. P., da Silveira, D. P., de Freitas, J. T. R., & da Silva, S. R. P. (2008). Evaporitos estratificados no Atlântico Sul: interpretação sísmica e controle tectono- estratigráfico na Bacia de Santos. In W. Mohriak, P. Szatmari, & S. M. C. Anjos (Eds.), *Sal: Geologia e Tectônica, Exemplos nas Basicas Brasileiras* (pp. 340–359). Beca Edições Ltda.

García-Senz, J. (2002). *Cuencas extensivas del Cretácico inferior en los Pirineos centrales, formación y subsecuente inversión* (PhD dissertation). University of Barcelona, Barcelona, p. 310.

Giles, K. A., Lawton, T., Shock, A., Kernen, R., Hearon, T., & Rowan, M. G. (2012). *A Halokinetic drape-fold model for Caprock in Diapir-flanking and subsalt positions*. AAPG Search and Discovery Article #40956, American Association of Petroleum Geologists.

Giles, K. A., & Rowan, M. G. (2012). Concepts in halokinetic-sequence deformation and stratigraphy. *Geological Society, London, Special Publications*, *363*(1), 7–31. https://doi.org/10.1144/SP363.2

Gottschalk, R. R., Anderson, A. V., Walker, J. D., Da Silva, J. C. et al (2004). Modes of contractional salt tectonics in Angola Block 33, Lower Congo Basin, West Africa. In P. Post (Ed.), *Salt-sediment interactions and hydrocarbon prospectivity: concepts, applications, and case studies for the 21st century: 24th Annual GCSSEPM Foundation Bob F. Perkins Research Conference* (pp. 705–734).

Graham, R., Jackson, M., Pilcher, R., & Kilsdonk, B. (2012). Allochthonous salt in the sub-Alpine fold–thrust belt of Haute Provence, France. *Geological Society, London, Special Publications*, *363*(1), 595–615. https://doi.org/10.1144/sp363.30

Granado, P., Roca, E., Strauss, P., Pelz, K., & Muñoz, J. A. (2019). Structural styles in fold-and-thrust belts involving early salt structures: The Northern Calcareous Alps (Austria). *Geology*, *47*, 51–54. https://doi.org/10.1130/G45281.1

Grasemann, B., Martel, S., & Passchier, C. (2005). Reverse and normal drag along a fault. *Journal of Structural Geology*, *27*, 999–1010. https://doi.org/10.1016/j.jsg.2005.04.006

Hazzard, R. T., Spooner, W. C., & Blanpied, B. W. (1947). Notes on the stratigraphy of the formations which underlie the Smackover Limestone in south Arkansas, northeast Texas, and north Louisiana. *Shreveport Geological Society 1945 Reference Report*, *2*, 483–503.

Hearon, T. E., Rowan, M. G., Giles, K. A., Kernen, R. A., Gannaway, C. E., Lawton, T. F., & Fiduk, J. C. (2015). Allochthonous salt initiation and advance in the northern Flinders and eastern Willouran ranges, South Australia: Using outcrops to test subsurface-based models from the northern Gulf of Mexico. *AAPG Bulletin*, *99*(2), 293–331. https://doi.org/10.1306/08111414022

Hearon, T. E. IV, Rowan, M. G., Lawton, T. G., Hannah, P. T., & Giles, K. A. (2015). Geology and tectonics of Neoproterozoic salt diapirs and salt sheets in the eastern Willouran Ranges, South Australia. *Basin Research*, *27*(2), 183–207. https://doi.org/10.1111/bre.12067

Hossack, J. (1995). Geometric rules of section balancing for salt structures. Salt Tectonics: A global perspective. *AAPG Memoir*, *65*, 29–40.

Hudec, M. R., & Jackson, M. P. A. (2007). Terra infirma: Understanding salt tectonics. *Earth-Science Reviews*, *82*(1–2), 1–28. https://doi.org/10.1016/j.earscirev.2007.01.001

Hudec, M. R., & Jackson, M. P. A. (2011). *The salt mine: a digital atlas of salt tectonics*. The University of Texas at Austin, Bureau of Economic Geology: Udden Book Series No. 5, AAPG Memoir 99. p. 305.

Izquierdo-Llavall, E., Roca, E., Xie, H., Pla, O., Muñoz, J. A., Rowan, M. G., Yuan, N., & Huang, S. (2018). Influence of overlapping décollements, syntectonic sedimentation, and structural inheritance in the evolution of a contractional system: The central Kuqa fold-and-thrust belt (Tian Shan Mountains, NW China). *Tectonics*, *37*(8), 2608–2632. https://doi.org/10.1029/2017tc004928

Jackson, C. A., Jackson, M. P., Hudec, M. R., & Rodriguez, C. (2014). Internal structure, kinematics, and growth of a salt wall: Insights from 3-D seismic data. *Geology*, *42*(4), 307–310. https://doi.org/10.1130/G34865.1

Jackson, C. A. L., Jackson, M. P., Hudec, M. R., & Rodriguez, C. R. (2015). Enigmatic structures within salt walls of the Santos Basin—Part 1: Geometry and kinematics from 3D seismic reflection and well data. *Journal of Structural Geology*, *75*, 135–162. https://doi.org/10.1016/j.jsg.2015.01.010

Jackson, C.-A.-L., & Lewis, M. M. (2012). Origin of an anhydrite sheath encircling a salt diapir and implications for the seismic imaging of steep-sided salt structures, Egersund Basin, Northern North Sea. *Journal of the Geological Society*, *169*(5), 593–599. https://doi.org/10.1144/0016-76492011-126

Jackson, M. P. A., & Cramez, C. (1989). Seismic recognition of salt welds in salt tectonics regimes. In Gulf of Mexico salt tectonics, associated processes and exploration potential: Gulf Coast Section SEPM Foundation 10th Annual Research Conference (pp. 66–71).

Jackson, M. P. A., & Hudec, M. R. (2017). *Salt tectonics*. Cambridge University Press. https://doi.org/10.1017/9781139003988

Jackson, M. P. A., Hudec, M. R., Jennette, D. C., & Kilby, R. E. (2008). Evolution of the Cretaceous Astrid thrust belt in the ultradeep-water Lower Congo Basin, Gabon. *AAPG Bulletin*, *92*(4), 487–511. https://doi.org/10.1306/12030707074

Jahani, S., Callot, J. P., Letouzey, J., & Frizon de Lamotte, D. (2009). The eastern termination of the Zagros Fold-and-Thrust Belt, Iran: Structures, evolution, and relationships between salt plugs, folding, and faulting. *Tectonics*, *28*. https://doi.org/10.1029/2008TC002418

Jenkins, R. J. F. (1990). The Adelaide fold belt: Tectonic reappraisal. In J. B. Jago, & P. S. Moore (Eds.), *The evolution of a Late Precambrian–Early Paleozoic rift complex: the Adelaide Geosyncline* (Vol. *16*, pp.

395–420). Geological Society of Australia Incorporated. Geological Society of Australia Special Publication.

Karner, G. D. (2000). Rifts of the Campos and Santos basins, southeastern Brazil: distribution and timing. In M. R. Mello, & B. J. Katz (Eds.), *Petroleum systems of south atlantic margins* (Vol. *73*, pp. 301–315). AAPG Memoir.

Kergaravat, C., Ribes, C., Callot, J. P., & Ringenbach, J. C. (2017). Tectono-stratigraphic evolution of salt-controlled minibasins in a fold and thrust belt, the Oligo-Miocene central Sivas Basin. *Journal of Structural Geology*, *102*, 75–97. https://doi.org/10.1016/j.jsg.2017.07.007

Kergaravat, C., Ribes, C., Legeay, E., Callot, J. P., Kavak, K. S., & Ringenbach, J. C. (2016). Minibasins and salt canopy in foreland fold-and-thrust belts: The central Sivas Basin, Turkey. *Tectonics*, *35*(6), 1342–1366. https://doi.org/10.1002/2016TC004186

Kernen, R. A., Giles, K. A., Poe, P. L., Gannaway Dalton, C. E., Rowan, M. G., Fiduk, J. C., & Hearon, T. E. (2019). Origin of the Neoproterozoic rim dolomite as lateral carbonate caprock, Patawarta salt sheet, Flinders Ranges, South Australia. *Australian Journal of Earth Sciences*, *67*(6), 815–832. https://doi.org/10.1080/08120099.2019.1588695

Kernen, R. A., Giles, K. A., Rowan, M. G., Lawton, T. F., & Hearon, T. E. (2012). Depositional and halokinetic-sequence stratigraphy of the Neoproterozoic Wonoka Formation adjacent to Patawarta allochthonous salt sheet, Central Flinders Ranges, South Australia. *Geological Society, London, Special Publications*, *363*(1), 81–105. https://doi.org/10.1144/SP363.5

Lemon, N. M. (1988). *Diapir recognition and modeling with examples from the late Proterozoic Adelaide Geosyncline, Central Flinders Ranges, South Australia* (Unpublished doctoral dissertation). University of Adelaide.

Lemon, N. M. (2000). A Neoproterozoic fringing stromatolite reef complex, Flinders Ranges, South Australia. *Precambrian Research*, *100*(13), 109–120. https://doi.org/10.1016/S0301-9268(99)00071-6

Li, J., Webb, A. A. G., Mao, X., Eckhoff, I., Colón, C., Zhang, K., Wang, H., Li, A., & He, D. (2014). Active surface salt structures of the western Kuqa fold-thrust belt, northwestern China. *Geosphere*, *10*, 1219–1234. https://doi.org/10.1130/GES01021.1

Medwedeff, D. A., & Suppe, J. (1997). Multibend fault-bend folding. *Journal of Structural Geology*, *19*(3-4), 279–292. https://doi.org/10.1016/S0191-8141(97)83026-X

Meisling, K. E., Cobbold, P. R., & Mount, V. S. (2001). Segmentation of an obliquely rifted margin, Campos and Santos basins, southeastern Brazil. *AAPG Bulletin*, *85*, 1903–1924.

Mendis, P. J. (2002). *The origin of the Geological Structures Diapirs, Grabens and Barite veins in the Flinders Range, South Australia* (PhD thesis). University of Adelaide, Adelaide, South Australia, p. 155.

Mount, T. J. (1975). *Diapirs and diapirism in the Adelaide 'Geosyncline,' South Australia* (PhD thesis). University of Adelaide, Adelaide, South Australia, p. 237.

Najafi, M., & Lajmorak, S. (2020). Contractional salt-tectonic system in the south Dezful embayment, Zagros. *Journal of Structural Geology*, *141*, 104204. https://doi.org/10.1016/j.jsg.2020.104204

Najafi, M., Vergés, J., Etemad-Saeed, N., & Karimnejad, H. R. (2018). Folding, thrusting and diapirism: Competing mechanisms for shaping the structure of the north Dezful Embayment, Zagros, Iran. *Basin Research*, *30*(6), 1200–1229. https://doi.org/10.1111/bre.12300

Parravano, V., Teixell, A., & Mora, A. (2015). Influence of salt in the tectonic development of the frontal thrust belt of the eastern Cordillera (Guatiquía area, Colombian Andes). *Interpretation*, *3*(4), SAA17-SAA27. https://doi.org/10.1190/int-2015-0011.1

Paul, E., Sandiford, M., & Flöttmann, T. (2000). Structural geometry of a thick-skinned fold-thrust belt termination: The Olary Block in the Adelaide Fold Belt, South Australia. *Australian Journal of Earth Sciences*, *47*(2), 281–289. https://doi.org/10.1046/j.1440-0952.2000.00779.x

Pichel, L. M., Finch, E., Huuse, M., & Redfern, J. (2017). The influence of shortening and sedimentation on rejuvenation of salt diapirs: A new discrete-element modelling approach. *Journal of Structural Geology*, *104*, 61–79. https://doi.org/10.1016/j.jsg.2017.09.016

Pla, O., Roca, E., Xie, H., Izquierdo-Llavall, E., Muñoz, J. A., Rowan, M. G., Ferrer, O., Gratacós, O., Yuang, N., & Huang, S. (2019). Influence of syntectonic sedimentation and décollement rheology on the geometry and evolution of orogenic wedges: Analogue modeling of the Kuqa fold-and-thrust belt (NW China). *Tectonics*, *38*(8), 2727–2755.

Preiss, W. V. (1987a). Stratigraphic nomenclature and classification. In W. V. Preiss (Ed.), *The Adelaide Geosyncline – Later Proterozoic stratigraphy, sedimentation, paleontology, and tectonics* (Vol. *53*, pp. 29–34). Geological Society of Australia Bulletin, Department of Mines and Energy, Geological Survey of South Australia.

Preiss, W. V. (1987b). Tectonics of the Adelaide Geosyncline. In W. V. Preiss (Ed.), *The Adelaide Geosyncline – Late Proterozoic stratigraphy, sedimentation, paleontology and tectonics* (Vol. *53*, pp. 255–281). Geological Society of Australia Bulletin.

Preiss, W. V. (1990). A stratigraphic and tectonic overview of the Adelaide Geosyncline, South Australia. In J. B. Jago, & P. S. Moore (Eds.), *The evolution of a Late Precambrian-Early Paleozoic rift complex: the Adelaide Geosyncline* (Vol. *16*, pp. 1–33). Geological Society of Australia Special Publication, Geological Society of Australia Incorporated.

Preiss, W. V. (1993). Delamerian orogeny. In J. F. Drexel, W. V. Preiss, & A. J. Parker (Eds.), *The geology of South Australia* (Vol. *1*). South Australia Geological Survey.

Preiss, W. V. (2000). The Adelaide Geosyncline of South Australia and its significance in Neoproterozoic continental reconstruction. *Precambrian Research*, *100*, 21–63. https://doi.org/10.1016/S0301-9268(99)00068-6

Preiss, W. V., & Cowley, W. M. (1999). Genetic stratigraphy and revised lithostratigraphic classification of the Burra {Group} in the Adelaide {Geosyncline}. *MESA Journal*, *14*, 30–40.

Preiss, W. V., Gostin, V. A., McKirdy, D. M., Ashley, P. M., Williams, G. E., & Schmidt, P. W. (2011). Chapter 69 The glacial succession of Sturtian age in South Australia: The Yudnamutana Subgroup. *Geological Society, London, Memoirs*, *36*(1), 701–712. https://doi.org/10.1144/M36.69

Ringenbach, J.-C., Salel, J.-F., Kergaravat, C., Ribes, C., Bonnel, C., & Callot, J.-P. (2013). Salt tectonics in the Sivas Basin, Turkey: Outstanding seismic analogues from outcrops. *First Break*, *31*, 93–101.

Rodriguez, C. R., Jackson, C. L., Rotevatn, A., Bell, R. E., & Francis, M. (2018). Dual tectonic-climatic controls on salt giant deposition in the Santos Basin, offshore Brazil. *Geosphere*, *14*(1), 215–242. https://doi.org/10.1130/GES01434.1

Roma, M., Vidal-Royo, O., McClay, K., Ferrer, O., & Muñoz, J. A. (2018). Tectonic inversion of salt-detached ramp-syncline basins as illustrated by analog modeling and kinematic restoration. *Interpretation*, *6*(1), T127–T144. https://doi.org/10.1190/INT-2017-0073.1

Rowan, M. G. (2017). Chapter 4: An overview of allochthonous salt tectonics. In J. I. Soto, J. F. Flinch, & G. Tari (Eds.), *Permo-Triassic Salt Provinces of Europe, North Africa and the Atlantic Margins* (pp. 97–114). https://doi.org/10.1016/B978-0-12-809417-4.00005-7

Rowan, M. G. (2020). Salt- and shale-detached gravity-driven failure of continental margins. In N. Scarselli, J. Adam, D. Chiarella, D. G. Roberts, & A. W. Bally (Eds.), *Regional geology and tectonics, volume 1: Principles of geologic analysis* (2nd ed., pp. 205–233). Elsevier.

Rowan, M. G., & Giles, K. A. (2020). Passive versus active salt diapirism. *AAPG Bulletin*, *105*, 53–63. https://doi.org/10.1306/05212020001

Rowan, M. G., Hearon, T. E. IV, Kernen, R. A., Giles, K. A., Gannaway-Dalton, C. E., Williams, N., Fiduk, J. C., Lawton, T. F., Hannah, A. H., & Fischer, M. P. (2019). A review of allochthonous salt tectonics in the Flinders and Willouran ranges, South Australia. *Australian Journal of Earth Sciences*, *67*(6), 787–813. https://doi.org/10.1080/08120099.2018.1553063

Rowan, M. G., Jackson, M. P. A., & Trudgill, B. D. (1999). Salt-related fault families and fault welds in the Northern Gulf of Mexico. *AAPG Bulletin*, *9*(9), 1–31.

Rowan, M. G., Lawton, T. F., Giles, K. A., & Ratliff, R. A. (2003). Near-salt deformation in La Popa basin, Mexico, and the northern Gulf of Mexico: A general model for passive diapirism. *AAPG Bulletin*, *87*, 733–756. https://doi.org/10.1306/01150302012

Rowan, M. G., Muñoz, J. A., Giles, K. A., Roca, E., Hearon, T. E. IV, Fiduk, J. C., Ferrer, O., & Fischer, M. P. (2020). Folding and fracturing of rocks adjacent to salt diapirs. *Journal of Structural Geology*, *141*, 104187. https://doi.org/10.1016/j.jsg.2020.104187

Rowan, M. G., Peel, F. J., & Vendeville, B. C. (2004). Gravity-driven fold belts on passive margins. In K. R. McClay (Ed.), *Thrust tectonics and hydrocarbon systems* (Vol. *82*, pp. 157–182). AAPG Memoir.

Rowan, M. G., & Ratliff, R. A. (2012). Cross-section restoration of salt-related deformation: Best practices and potential pitfalls. *Journal of Structural Geology*, *41*, 24–37. https://doi.org/10.1016/j.jsg.2011.12.012

Rowan, M. G., & Vendeville, B. C. (2006). Foldbelts with early salt withdrawal and diapirism: Physical model and examples from the northern Gulf of Mexico and the Flinders Ranges, Australia. *Marine and Petroleum Geology*, *23*(9–10), 871–891. https://doi.org/10.1016/j.marpetgeo.2006.08.003

Rubinat, M. (2012). *Basement fault influence on the Bicorb-Quesa Salt Wall kinematics, insights from Magnetotelluric and Paleomagnetic techniques on Salt Tectonics* (PhD dissertation). University of Barcelona, Barcelona. https://www.tdx.cat/handle/10803/84162#page=1

Salvador, A. (1987). Late Triassic-Jurassic paleogeography and origin of Gulf of Mexico basin. *AAPG Bulletin*, *71*, 419–451.

Sánchez Rivera, R., Cruz Mercado, M. Á., Reyes Tovar, E., López Céspedes, H. G., Peterson Rodriguez, R. H., Flores Zamora, J. C., León Ramirez, R., & Barrera González, D. (2011). Tectonic evolution of the South Gulf Salt Province in the Gulf of Mexico. *Gulf Coast Association of Geological Societies Transactions*, *61*, 421–427.

Sandiford, M., Paul, E., & Flottmann, T. (1998). Sedimentary thickness variations and deformation intensity during basin inversion in the Flinders Ranges, South Australia. *Journal of Structural Geology*, *20*(12), 1721–1731. https://doi.org/10.1016/S0191-8141(98)00088-1

Saura, E., Ardèvol i Oró, L., Teixell, A., & Vergés, J. (2016). Rising and falling diapirs, shifting depocenters, and flap overturning in the Cretaceous Sopeira and Sant Gervàs subbasins (Ribagorça Basin, southern Pyrenees). *Tectonics*, *35*(3), 638–662. https://doi.org/10.1002/2015TC004001

Saura, E., Vergés, J., Martín-Martín, J. D., Messager, G., Moragas, M., Razin, P., Grélaud, C., Joussiaume, R., Malaval, M., Homke, S., & Hunt, D. W. (2014). Syn- to post-rift diapirism and minibasins of the Central High Atlas (Morocco): The changing face of a mountain belt. *Journal of the Geological Society*, *171*(1), 97–105. https://doi.org/10.1144/jgs2013-079

Sprigg, R. C. (1952). Sedimentation in the Adelaide Geosyncline and the formation of a Continental terrace. In M. F. Glaessner, & E. A. Rudd (Eds.), *Sir douglas mawson anniversary volume* (pp. 153–159). University of Adelaide.

Suppe, J. (1983). Geometry and kinematics of fault-bend folding. *American Journal of Science*, *283*, 684–721. https://doi.org/10.2475/ajs.283.7.684

Suppe, J. (1985). *Principles of structural geology*. Prentice Hall.

Thomson, B. P. (1969). Palaeozoic era. In L. W. Parkin (Ed.), *Handbook of South Australian geology* (pp. 97–108). Geological Survey of South Australia.

Turner, S., Haines, P., Foster, D., Powell, R., Sandiford, M., & Offler, R. (2009). Did the delamerian orogeny start in the neoproterozoic? *The Journal of Geology*, *117*(5), 575–583. https://doi.org/10.1086/600866

Vendeville, B. C., & Nilsen, K. T. (1995). Episodic growth of salt diapirs driven by horizontal shortening, in salt, sediment, and hydrocarbons. Society of Economic Paleontologists and Mineralogists Gulf Coast Section, 16th annual research conference program and extended abstracts. 285–295.

Vergés, J., Moragas, M., Martín-Martín, J. D., Saura, E., Casciello, E., Razin, P., & Hunt, D. W. (2017). Salt Tectonics in the Atlas Mountains of Morocco. *Permo-Triassic Salt Provinces of Europe, North Africa and the Atlantic Margins*, *2014*, 563–579. https://doi.org/10.1016/B978-0-12-809417-4.00027-6

Wagner, B. H., & Jackson, M. P. A. (2011). Viscous flow during salt welding. *Tectonophysics*, *510*(3–4), 309–326. https://doi.org/10.1016/j.tecto.2011.07.012

Warsitzka, M., Kley, J., & Kukowski, N. (2015). Analogue experiments of salt flow and pillow growth due to basement faulting and differential loading. *Solid Earth*, *6*, 9–31. https://doi.org/10.5194/se-6-9-2015

Webb, B. P. (1960). Diapiric structures in the Flinders Ranges, South Australia. *Australian Journal of Science*, *22*, 390–391.

William, N. J., Fischer, M. P., & Canova, D. P. (2019). Structural evolution and deformation near a tertiary salt weld, Willouran Ranges, South Australia. *Marine and Petroleum Geology*, *102*, 305–320. https://doi.org/10.1016/j.marpetgeo.2018.12.035

How to cite this article: Vidal-Royo, O., Rowan, M. G., Ferrer, O., Fischer, M. P., Fiduk, J. C., Canova, D. P., Hearon, T. E. IV, & Giles, K. A. (2021). The transition from salt diapir to weld and thrust: Examples from the Northern Flinders Ranges in South Australia. *Basin Res*, 00, 1–30. https://doi.org/10.1111/bre.12579